NTNU
Norwegian University of
Science and Technology

Monte Carlo simulations to probe gel-nanoparticle interfaces using restricted polymers to mimic surface topologies

Nicholas Christiansen

Master of Science in Physics and Mathematics
Submission date: August 2018
Supervisor: Rita de Sousa Dias, IFY

Norwegian University of Science and Technology
Department of Physics

Abstract

The use of silica nanoparticles as an adhesive mediator in hydrogels and suturing of wounds, has been of interest. This thesis investigates the mode of interaction between nanoparticles and a polymer network interface, where the latter is approximated using a simple chain system with varying degrees of restrictions. The idea is that restricting one end should mimic a loose chain on the surface of a gel, while restricting two ends is similar to that of an internalized polymer. The strength of the attractive potential is varied throughout the work.

As would be expected, chains with a fixed end (one node system) show similar interactions with a nanoparticle when compared to free chains. Chains that have both ends restricted and loose or restricted middle monomers (two and three node systems, respectively) show a similar behavior to that of the 1 node systems in the presence of a NP, for short node separations. With increasing node separation, mimicking the swelling of a hydrogel, the two and three node systems show lower sensitivity, in regards to the number of and length of tails, trains and loops, to increasing potentials.

For the three node system there is a clear preference for the nanoparticle to adsorb to the central node for node separations smaller than the range of the interacting potential of the nanoparticles. As the node separations increase, the three node system is similar to that of the two node system, with the nanoparticles preferring to adsorb to the center of the polymer chains.

Sammendrag (Norwegian Abstract)

Bruken av nanopartikler av silisiumoksid som lim i hydrogeller, og som festemiddel i sår, har den siste tiden vært av interesse. Denne oppgaven undersøker hvordan nanopartiklene av silisiumoksid interagerer med et polymernettverk sin overflate. Dette gjøres ved å tilnærme overflaten av polymernettverket med en enkel polymer, med varierende grad av restriskjoner. Idéen er at restriskjonen i en ende av polymeret (node) ligner løse polymerer på overflaten av et polymernettverk, og polymerer med to ender festet, ligner interne polymerer. Styrken på de attraktive kreftene har blitt variert gjennom arbeid.

Som forventet, viste en polymer med en ende festet like interaksjoner med nanopartikkelen sammenlignet med en fri polymer. For polymeret med begge ender festet, og festet eller ikke festet midtpunkt, var det en lignende interaksjon med nanopartiklen for små separasjoner av nodene. Ved større separasjon, gjort for å etterligne svellingen i en hydrogel, viste systeme med to og tre noder lavere sensitivitet med tanke på endring i antall og lengde av haler, sløyfer og tog, for økende attraktiv potensial.

For systemet med tre noder var det en klar preferanse for nanopartikkelen å adsorbere til den midterste noden for separasjoner av nodene lavere enn rekkevidden på det interagerende potensialet. For større separasjoner viste dette systemet lignende tendenser som systemet med to noder, og viste en klar preferanse for å adsorbere til midten av en av polymeren fremfor noden.

Preface

This thesis is written and handed in as a part of the course TFY4590 - Biophysics, Master Thesis. It is the result of my final work for my degree as a Master of Science in Physics and Mathematics at the Department of Physics (IFY) at the Norwegian University of Science and Technology. The work was done during the spring and summer of 2018.

I would like to thank my supervisor, Rita de Sousa Dias, for excellent guidance and help throughout the work. I would also like to thank Morten Stornes for useful feedback during the process, as well as valuable and interesting discussions.

Nicholas Christiansen
Trondheim, August 2018

Contents

List of Figures

List of Tables

Abbreviations

CAM	cell adhesion molecule
CMS	colloidal mesoporous silica
ECM	extracellular matrix
LJ	Lennard-Jones potential
MC	Monte Carlo
MD	molecular dynamics
MSN	mesoporous silica nanoparticle
NP	nanoparticle
PAAm	polyacrylamide
PDMA	poly(dimethylacrylamide)
PNIPA	Poly(N-isopropylacrylamide)
vdW	van der Waals

Chapter 1

Introduction

The use of nanoparticles (NPs) for medical purposes has increased over the past few decades, with a wide variety of uses ranging from targeted drug and gene delivery, as fluorophores and contrast agents for medical imaging (Murthy 2007). Recently the use of silica (SiO_2) NPs as mediators for gluing gels and medical devices to tissue, as well as wound closure, has been studied (Rose et al. 2014). Using silica NPs in wet solution, it was proven possible to glue two slabs of poly(dimethylacrylamide) (PDMA) gels, and a lack of adhesion when trying to glue polyacrylamide (PAAm) gels. Meddahi-Pellé et al. (2014) demonstrated that it was possible to use silica NPs in solution as an adhesive when gluing skin wounds in rats. Compared to traditional suturing methods, the NP solution showed a better rate of wound healing. In addition NP solutions were found to have hemostatic capabilities and a possble use as adhesives for gluing medical devices to internal organs.

In a more recent study, Perrin et al. (2018) investigated the dynamics of coarse-grained PAAm and PDMA polymers near a silica surface using molecular dynamics (MD) simulations. They found that water screens the

interactions between the surface of the NP and polymer chain. Additionally, the water molecules compete with the adsorption of the polymers to the silica surface, playing a steric role. The steric effect of the water molecules was found to be more prominent in the PAAm system than in the PDMA system, yielding one explanation as to why the adhesion between silica NPs is favoured in the latter compared to the prior system. Other studies have criticized the use of silica NPs, finding that the inorganic base used in the solution, NaOH and KOH, plays a significant role on adhesive properties of the solution, and that these on their own, display an adhesive capability five times stronger than that of the spherical silica NPs (Liu et al. 2017).

Even so, silica NPs have many interesting aspects. In addition to working as an adhesive mediator, the mesoporous silica nanoparticles (MSNs) can be used to load drugs to increase the healing rates of wounds and decrease bacterial growth, as well as having a highly tunable degradation period and adhesive capabilities (Choi et al. 2015, Hao et al. 2012). Other NPs than silica have been studied. Zinc oxides (ZnO) and iron oxide (Fe_2O_3) NPs as adhesive mediators have shown reduced bacterial growth and similar or better adhesive properties as the silica NPs (Annabi et al. 2014, Gao et al. 2017). Nevertheless, silica NPs are preferred because of the aforementioned reasons.

1.1 Medical interest

Good medical adhesives should display strong adhesive capabilities, low toxicity and reduce microbial growth, as well as be cheap and easy to apply. In addition, they should work as local depots for releasing therapeutic medicine to increase wound healing and trigger repair. Such a use

has been demonstrated using a fibrous layered matrix as an adhesive with a complex scaffolding to deliver a drug, but these are complex materials and hard to produce (Yoon et al. 2016). Compared to traditional suturing methods, the use of NPs could be used as a non-invasive method to suture wounds in surgical applications, glue medical devices and work as a hemostatic agent. They are easier to apply in wet conditions, cheap to produce, and degrade naturally in physiological conditions (Choi et al. 2015). Traditional suturing methods using staples, wires or inorganic glues are often harmful to the body and increase the risk of infection or foreign body reactions (Annabi et al. 2014). Synthetic glues show a high cure rate, but cannot be used in wet environments, making them hard to apply. Natural surgical materials work as barriers against pathogens, are pro-inflammatory and degrade naturally over time, while foreign objects such as staples have to be removed. Natural adhesives, on the other hand, are expensive to produce and have a limited availability, making them less attractive.

It is assumed that silica NPs either interact with the surface structures of the extracellular matrix (ECM), or the cell membrane. The lipid bilayer constituting the cell membrane is embedded with different types of cell adhesion molecules (CAMs). The CAMs allow cells of different types to adhere to each other (Hardin & Bertoni 2015, Chapter 17). NPs presumably bridge between two cell membranes, and have been shown to produce a similar effect between cells as CAMs Brunel et al. (2016). NPs have been shown to be internalized in the cell through energy dependent pathways, as well as stick to the surface Lesniak et al. (2013). NPs have also been shown to induce structural changes in vesicles Noguchi & Takasu (2002).

Regarding cytotoxicity, silica NPs have been shown to induce necrosis

through apoptosis in certain intestinal cells when used as food additives (Devasena 2016, Chapter 5). They have also been found to be less toxic than SiO_2 nanowires in cultured human cells (Adili et al. 2008) and *in vitro* studies have shown that amorphous silica particles induce apoptosis and disrupt certain cell processes (Moia 2015). Li et al. (2015) found that the size and shape of MSNs affect the uptake in the small intestine, and therefore also toxicity, when administered orally. This is also shown for endothelial cells, where decreasing size and increasing the dose of monodisperse amorphous silica NPs, decreases cell viability (Napierska et al. 2009). Wu et al. (2011) displayed little change to the brain and behaviour of rats when administering silica NPs. Further *in vitro* studies indicated an accumulation in the G2 and M phase of the cell cycle, and therefore some potential risk to neurodegenerative disorders. Huang et al. (2010) showed that the impact on different aspects of cellular function, including cell proliferation, apoptosis, cytoskeleton formation, adhesion and migration, depends greatly on the aspect ratio of silica NPs, where elongated NPs showed the greatest negative impact. On the other hand, Kim et al. (2017) observed no cytotoxicity, and the full effect on cells is not yet fully researched. Thus the issue of silica NPs cytotoxicity should be considered a topic for further investigation and interest.

1.2 Polymer adsorption to surfaces

As stated above, there is some controversy as to the exact type of interaction between the gels investigated and the silica NPs in aqueous suspension. Rose et al. (2014) proposed that the silica NPs work as a nanobridge between the two networks, and that the polymers in the network adhere to the surface of the silica NPs by forming multiple loops and trains across

it. Another possibility is that the polymers stretch across the layer formed by the NPs and entangle in the opposing gel. Assuming that the silica NPs and gels have no charge interaction, the adhesion to the surface by the polymer may be thermally driven. The strength of the interaction between the NPs and polymer must be larger than that of the lost conformational entropy of the polymer, and therefore thermodynamically viable (Cosgrove 2010, Chapter 8).

The entropy of polymer chains and their interaction when adsorbing to large surfaces has been studied thoroughly over the past decades, both experimentally and through computer simulations. The basis for most of the work which has been done was proposed by Flory (1953), with an easy to comprehend lattice model for polymer mixtures which has been further tested using Monte Carlos (MCs) simulations (Sariban & Binder 1987). A statistical analysis of polymer monolayers using this theory has also been investigated (Simha et al. 1953). Other work includes a lattice Monte Carlo study of long chain conformations at solid–polymer melt interfaces, which found some discrepancies in Flory-Huggins model of the first order Bitsanis & Brinke (1993). The study of adsorption to a plane has been done using MDs simulations as well, in addition to experimental work showing the adhesion and loop formation of polymer adsorption to a SiO_2 surface by hydrogen bonding Guzman et al. (2011).

Fleer & Scheutjens (1982) found that in bulk polymer the chains would essentially have two tails of one third of the monomers each, using MC simulations. Dilute systems have short trains and long loops, in addition to long tails. The length of the tail hardly decreases with an increase in weight, and the relationship between tail length and chain length is nearly linear (Scheutjens & Fleer 1980). Similar findings were shown by Welch et al. (2015) for semi-flexible filaments through both experimental

studies and computer simulations. Flexible polymers tend to form loops along a surface while stiff polymers prefer to form longer tails. For a system containing both stiff and flexible chains, Källrot & Linse (2010) found that the stiff and long chains dictate the adsorption behaviour at the surface and that stiff and long polymers will replace short and stiff polymers at the surface. They also found that the stiffness of the chains had a large impact on the fraction of polymers in tails and trains.

The study of polymer adhesion to spherical NPs yields similar results, but the difference between a flat surface and solid sphere should be viewed with interest. As the polymer chains can wrap around the spherical NPs the loss in conformational entropy will be larger than when adsorbing to a surface (Thompson et al. 2001). For polymers of varying stiffness, Song et al. (2018) found that as the chain stiffness is increased they will transition from a helical structure to a tangent on the surface, with the NP adsorbed close to the middle of the chain. Similar results have been found by Stornes et al. (2017) when studying weak polyacids adsorbing on a charged NP. At the endpoints of a polyacid the contact probability was lower than that at the center of the polyacid.

Smith et al. (2003) looked into the interaction between bulk polymer and a NP matrix. When the interaction strength between the NPs and polymers were weak there was an aggregation of the NPs. Increasing the interaction strength the between NPs and polymers indicated a dispersion of the NPs as the polymers forced themselves between the NPs, adsorbing to the surface of these. This creates an adhesion of the polymer to two NPs, which could prove feasible for loose ends in a hydrogel.

Other studies have focused on the adhesive properties of NPs in terms of available interacting area on the surface of the silica NPs. Kim et al. (2017) studied the effect of grooves on colloidal mesoporous silica (CMS),

showing that an increase in surface area (more golf ball like particles) increased the adhesion up top 1.8 times larger when compared to that of the nonporous silica NPs. They also studied the effect of concentration variations, showing an increasing adhesion until a peak was found and a subsequent lowering of adhesive abilities, with increasing NP concentration.

1.3 Approach

For simplicity, most of the reported MC studies use the Lennard-Jones potential (LJ)-potential to describe weak, non-covalent, van der Waals (vdW) forces between polymer chains and a chosen surface. These interactions normally have bond energies ranging from 0.1 to 10 $\mathrm{kJ\,mol^{-1}}$ (Næss et al. 2016).

In this thesis, we use coarse-grained MC simulations to look into the adsorption behaviour of polymer-NPs complexes and NP interaction with a small polymer network. The main goal is to get an understanding of the effects of loose ends versus connected ends of polymers in gels. Four simple systems are tested, in addition to a reference system. The systems consist of a polymer with one, two or three nodes which do not move under simulation, as well as a simple polymer network. The reference system consists of a single polymer with no fastened ends. To run the simulations, the software *MOLSIM*, is used (Reščič & Linse 2015).

To probe this interaction a LJ 6-12 potential has been used to approximate the weak vdWs interactions between the NP and polymer chains. The strength of the potential is varied, as well as the node separation, where this is applicable. For simplicity and generality, we disregard the charge of the silica, even though a theory for the charge dependence of

silica NPs on size and pH is readily available (Barisik et al. 2014).

This work is organized as follows. Chapter 2 presents a brief introduction to the structure and theory of gels, as well as the model used. Chapter 3 presents the systems used, and different input parameters. In chapter 4, the results are presented and discussed. A summary and closing remarks are given in Chapter 5.

Chapter 2

Theory

The following chapter focuses on aspects related to gels, as well as the model used in the simulations. The theory on gels is not explicitly used. Even so, an understanding of the nature of different types of gels, and their topology is needed to gain insight into the nature of the basic model which is used in the simulation.

2.1 Gels

Based on the type of interactions between the polymers constituting a gel, they may be categorized differently. Strong gels are formed by the mutliple polymers being linked at relatively few points through covalent bonds. This creates a network which requires a lot of energy to break the bonds (Treloar 2005). Biopolymer gels often form entanglement networks, such as polysaccharide gels, which form when the polymers in a solution entangle after the concentration of polymers in a solution exceeds a critical point (Clark & Ross-Murphy 1987). The polymers will twist on themselves as they entangle, making them hard to separate even as the system

is diluted. Weak gels are made from polymers forming gels upon reaching a critical concentration, where the interaction is governed by weak interactions such as hydrogen bonding. These bonds will form, break and reform in a dynamic way, and if the gel is diluted it will transition back into a polymer melt.

Weak gels will behave like strong gels under certain circumstances, but fail at others. For example, they will rupture and fail as they go beyond their ultimate strain for high frequencies in rheological experiments, in a similar fashion as strong gels, but will flow like liquids at low frequencies (Clark & Ross-Murphy 1987).

The effect of adding clay composites to different gels has also been studied to a wide extent (Theng 1982). Adding clay to gels changes the conformation of the polymers in the gel, as well as multiple traits of the gels (Shibayama et al. 2004, Haraguchi & Li 2006, Shibayama et al. 2004). For instance, Haraguchi (2007) showed that adding clay composites to Poly(N-isopropylacrylamide) (PNIPA) increased self crosslinking, added softness, durability, rigidity, elongation and recovery. Adding clay composites indicates that a wide variety of tuning abilities are available when changing the crosslinking nature and density and self adhesion of the polymers in a gel. PNIPA hydrogels are of special interest as they have many similar traits to biological gels, with traits that reach their critical point near similar conditions as in the human body.

In the human body, cells are suspended in extracellular fluid and surrounded by a matrix (the ECM) consisting of different polymers depending on the type of cell. The ECM is used by cells to migrate, and is secreted by the cells themselves to stabilize their surroundings. The ECM is generally constituted by three types of molecules. These are adhesive glycoproteins, structural proteins, and protein-polysaccharide complexes

(proteoglycans). The ECM is formed by proteoglycans, and adhesive glycoproteins such as laminins and fibronectins allow the cells stick to the matrix. Structural proteins, mainly made up of elastins and collagen, give the ECM flexibility and strength. Elastins consist of glycine covalently linked to non-hydroxylated proline residues Nelson & Cox (2013). Collagen fibres, which creates the elasticity in the skin, surround epithelial cells, and a rigid ECM made of cartilage surrounds bone cells (Hardin & Bertoni 2015, Chapter 17). Thus the gel-like properties, a well as chain stiffnes and charge, of different types of tissue will vary greatly, as stated by Christiansen (2017).

2.2 Conformational Entropy of Polymers

The conformational entropy of a polymer can be given as a simple equation using the third law of thermodynamics. The entropy, S, of a polymer can be written as

$$S = k_B \ln W, \tag{2.1}$$

where W is the number of possible conformations for the polymer chain, and k_B is the Boltzmann constant (Cosgrove 2010). Given that the chain has three possible spatial orientations when free and only two when fully adsorbed to a surface, we can assume that the chain has 3^n number of conformations when free in solution and 2^n when fully adsorbed. Equation 2.1 can then be written as

$$S = k_B \ln \frac{2^n}{3^n}. \tag{2.2}$$

This equation is a rough estimate at best, as it disregards the effects of

solvent molecules, but may still serve as a useful indication of the loss of entropy as chains adsorb onto a surface.

Rewriting equation 2.1, we get

$$S = -0.4\ k_B n, \tag{2.3}$$

suggesting that the interacting potential between a polymer chain and a surface must be larger than $0.4k_BT$, where T is the temperature in the system, and k_BT the thermal energy.

2.3 Potential Energy

To study the interactions for a polymer chain adsorbing to a NP we consider a simple model. The total energy in the system, U, is given by the equation

$$U = U_{\text{nonbond}} + U_{\text{bond}} + U_{\text{ang}}. \tag{2.4}$$

The interactions between non bound monomers in the system are represented by U_{nonbond}. U_{nonbond} is given by

$$U_{\text{nonbond}} = \sum_{i<j} u_{ij}(r_{ij}), \tag{2.5}$$

where the non bound potential is found as a summation over all interacting pairs through the individual potentials $u_{ij}(r_{ij})$ between particles i and j, as a function of the center to center distance, r_{ij}.

The model chosen for the value of the interacting potential is the LJ 6-12 potential. This potential is given by the equation

$$u_{ij}(r_{ij}) = 4\varepsilon\left[\left(\frac{\sigma}{r_{ij}}\right)^{12} - \left(\frac{\sigma}{r_{ij}}\right)^{6}\right], \tag{2.6}$$

which can be seen in figure 2.1. Here r_{ij} is the center to center distance between interacting particles, ε is the strength of the potential well, r_{min} is the distance to the minimum of the potential and σ is the distance at which the potential is zero.

Solving the LJ potential for $u_{ij} = 0$, the relation between σ and r_{min} is found. This yields the equation

$$\sigma = \frac{1}{\sqrt[6]{2}}\, r_{\text{min}}. \tag{2.7}$$

The distance to r_{min} should, according to the *MOLSIM* manual, be chosen so that it is approximately $4/3 \times r_{ij}$, where r_{ij} is the distance between the centers of the interacting particles i and j.

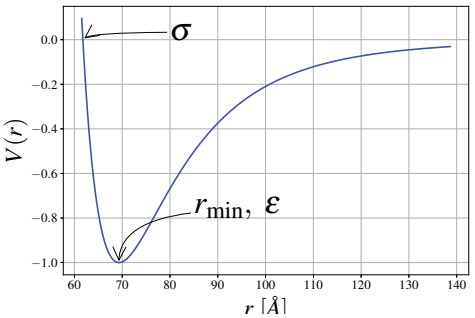

Figure 2.1: The Lennard-Jones 6-12 potential with the distance σ at which the potential crosses zero along the x-axis, the distance r_{min} to the potential well and ε the depth of the well.

The bonding energies, U_{bond}, for bonds in a chain, is given by

$$U_{\text{bond}} = \frac{k_{\text{bond}}}{2} \sum_{i=1}^{N_{\text{bond}}} (r_i - r_0), \tag{2.8}$$

where k_{bond} is the bond force constant. The summation is done over all N_{bond} bonds i in a chain. The equilibrium bond length is given by r_0 and the bond length i between two adjacent monomers along a chain is r_i. All chains in a system are evaluated.

The angular momentum, U_{ang}, of the chain is given by the equation

$$U_{\text{ang}} = \frac{k_{\text{ang}}}{2} \sum_{i=1}^{N_{\text{ang}}} (\alpha_i - \alpha_0). \tag{2.9}$$

Again the summation is done over all interacting pairs in all chains. The angular force constant is k_{ang}, α_i is the angle formed between adjacent particles in a chain and α_0 is the equilibrium angle for the system. The total number of angles to be considered is given by N_{ang}.

The radius of gyration, R_g, is the radius spanned by a polymer chain when it is in a coil conformation, describing the spatial dimension of the chain (Næss et al. 2016). A common measure for the average R_g is given by

$$\langle R_g^2 \rangle = \frac{\langle \sum_{i=1}^{N_{\text{mon}}} |r_i - r_{\text{cm}}|^2 \rangle}{N_{\text{mon}}}. \tag{2.10}$$

The summation is done over all monomers i in a chain. Here, r_{cm} is the position of the center of mass for the chain and r_i is the position of monomer i. The value is normalized with respect to the total number of monomers, N_{mon}.

The end-to-end distance R_{ee}, gives a measure of the distance between two ends along a polymer chain. The average R_{ee} is given by

$$\langle R_{ee}^2 \rangle = \langle |r_{N_{\text{mon}}} - r_1|^2 \rangle, \tag{2.11}$$

where r_1 and $r_{N_{\text{mon}}}$ are the positions of the first and last monomer along a polymer chain, respectively.

Chapter 3

Method

To probe the interaction between silica NP and gels, and how the surface topology of gels may affect this interaction, MC simulations of a coarse grained model describing polymer chains, network and a NP have been used. The polymers are modelled using a spring-bead model, and the NP was modelled as a sphere. The beads (monomers) used in the polymer chains were modelled as spheres, and one monomer is equal to one segment of the chain. All spheres were modelled with hard sphere boundaries. This creates a strong repulsion at the radius of the sphere, hindering the spheres from overlaping. For the polymer network, a diamond lattice was implemented. All runs were done in the canonical (NVT) ensemble, with a constant volume, temperature and number of particles throughout all the runs. For all systems, a spherical simulation cell with closed boundaries was utilized. The radius, r_{cell}, of the spherical cell was set to 600.0 Å. Two main systems were studied. In the first, simple models are taken to asses the effect of tails and nodes on the interaction of NPs with polymer networks, and were constituted by one NP and one chain that is free (reference system), or has one, two or three monomers which were fixed (1

node, 2 node and 3 node system, respectively). The second main system corresponds to a small polymer network and one NP.

An equilibrium run and subsequent production run was done for all systems. For each run, $n_1 \times n_2$ steps are made, and the results are given as an average over the production runs. The number of steps for each run, together with an overview of all the systems, can be found in Table 3.1. For each MC step one trial move is attempted per particle in the system. A trial move is either accepted or rejected based on whether or not a move is viable in consideration to potential energies in the system given by Equation 2.4 and steric repulsion such as hard sphere overlap.

Table 3.1: Systems used to probe the NP adhesion to different chain configurations by MC simulations. The first n_1 and n_2 for each system denotes the equilibrium run, while the second is that for the production run. All systems are run $n_1 \times n_2$ times. For the polymer chains with nodes, the nodes are evenly spaced at the beginning, middle and ends of the N_{mon} in a chain.

System	Configuration	N_{mon}	n_1	n_2
Reference	free chain	61	1000	35000
			1000	45000[a]
1 node	one end stuck	61	1000	35000
			1000	45000[a]
2 node	both ends stuck	62	100	35000
			100	45000
3 node	both ends, and middle stuck	123	100	35000
			100	45000
Polymer network	diamond lattice	9	50	60000
			100	20000[b,c]

[a] Additional runs for theses systems of $n_1 = 100$ and $n_2 = 45000$ were done for loop-tail-train statistics.
[b] For $\varepsilon/k_BT = 0.0$, the $k_{\text{ang}} = 1.0\,\text{kJ}\,\text{mol}^{-1}$ was done with 50×20000 and 100×20000 steps.
[c] For $\varepsilon/k_BT = 1.0$, the $k_{\text{ang}} = 1.0\,\text{kJ}\,\text{mol}^{-1}$ was done with 50×10000 and 100×10000 steps.

For the reference and 1 node systems, a single polymer chain of 61 monomers was used. In the reference system, all of the monomers in the chain could move, while the first monomer, the node, in the 1 node system was set to have zero probability of moving for any given step. The 2 node system consisted of a 62 monomer chain, configured as two nodes at either end of a 60 monomer chain. Similarly, the 3 node system consisted of a chain with a total of 123 monomers, with an alternating structure of one node and a 60 monomer freely moving chain part. All systems were configured in a helical configuration at step zero. This was done to ensure that the nodes were on the same axis, as well as to avoid hard sphere overlap when setting up the systems for simulation. The initial configuration for all systems can be seen in Figure 3.1. The NP was set at a random position inside the spherical cell.

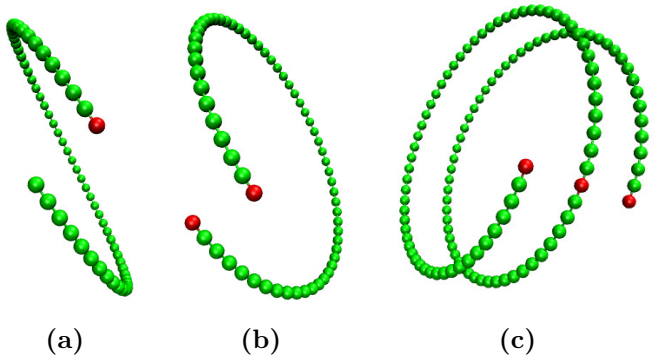

Figure 3.1: Snapshots of the initial configuration of the reference and 1 node systems (a), the 2 node system (b) and 3 node system (c). Nodes are colored red, while monomers that are allowed to move during the simulation are colored green.

The radius of the monomers, r_{mon}, was 2.0 Å, and the radius of the NP,

r_{NP} , was 50.0 Å. Force constants for the bond potential, k_{bond}, and angular potential, k_{ang}, were 2.4088 kJ mol^{-1} and 0.002 kJ mol^{-1}, respectively. The simulations were done at conditions approximately at room temperature and with normal atmospheric pressure. All chosen parameters can be seen in Table 3.2. These were held constant for all polymer chain systems. Some changes were made for the polymer network, as indicated below.

Table 3.2: Table containing variable parameters held constant for all simulations, unless otherwise specified.

Parameter	Symbol [Units]	Value
Temperature	T [K]	298.0
Radius of spherical simulation cell	r_{cell} [Å]	600.0
Radius of chain monomer	r_{mon} [Å]	2.0
Radius of nanoparticle	r_{NP} [Å]	50.0
Thermal energy	k_BT [kJ mol^{-1}]	2.48
Force constant of bond potential	k_{bond} [kJ mol^{-1}]	2.4088
Force constant of angle potential	k_{ang} [kJ mol^{-1}]	0.002
Equilibrium separation for bond potential	r_0 [Å]	5.0
Equilibrium angle for angle potential	α_0 [°]	180.0
NP-monomer LJ parameter	σ [Å]	61.7
Adsorbing distance	r_{contact} [Å]	70.0

To choose the LJ parameter σ, equation 2.7 was used. The distance, r_{min}, to the minimum of the potential well was determined as instructed in the *MOLSIM* manual, yielding a value of $\sigma = 61.7$ Å. The value for the adsorbing distance, r_{contact}, of a monomer in the chains to the NP was chosen carefully. The segments in a chain will adsorb to the NP at the distance corresponding to distance of the minimum of the potential well, but will not reach the surface of the NP. This means that the chains will be able to fluctuate on either side of the potential minimum. The ratio

between contact distance and minimum of the potential well, and effect on contact probability is shown in Figure 3.2. Note the end effects of the polymer chain for the ratio $r_{\text{contact}}/r_{\text{min}} = 1.0$. The adsorbing distance must be large enough to encompass the distance to the minimum of the LJ potential, and not so large that it counts too many particles as adsorbed. Here a contact distance of 70.0 Å was chosen, which corresponds to a ratio of $r_{\text{contact}}/r_{\text{min}} = 1.03$.

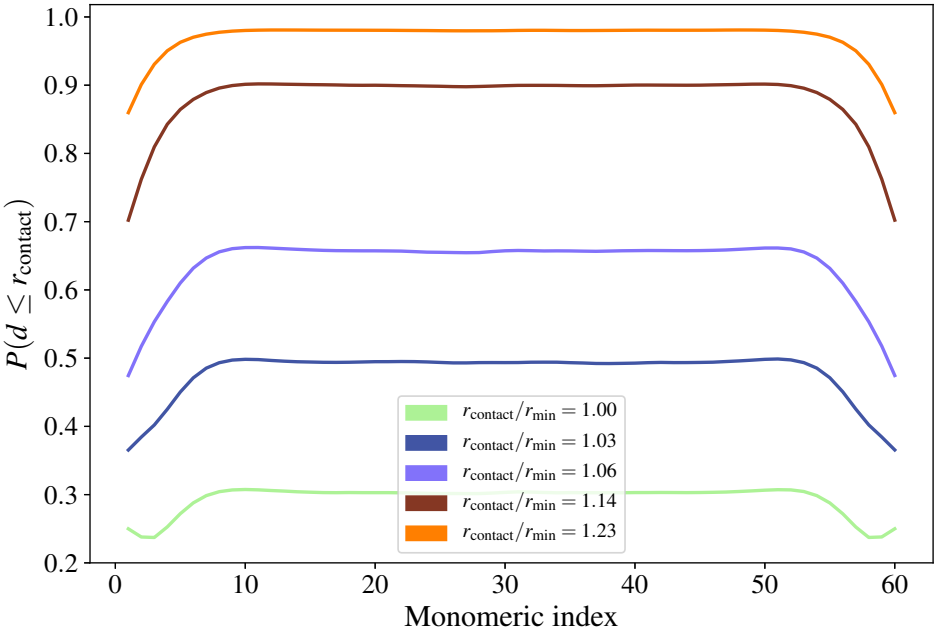

Figure 3.2: Probability, $P(d \leq r_{\text{contact}})$, of finding a monomer along the chain at a distance d less than or equal to r_{contact} for different contact values when using a Lennard-Jones potential potential. Note the increase in contact probability for the first and last monomer for $r_{\text{contact}}/r_{\text{min}} = 1.00$. The strength of the potential used is $\varepsilon/k_B T = 1.0$

For all NP-polymer systems, the strength of the interaction, ε, was varied. In addition, for 2 node and 3 node systems, the node separation

was also investigated. The values used can be seen in Table 3.3. Increasing the node separation is assumed to be equivalent to a gel swelling.

Table 3.3: Parameters used for simulations on single NP interaction with chains with variable degree of mobility. ε/k_BT is the interacting potential for the Lennard-Jones potential potential, and s the separation between nodes.

Parameter	Value
ε/k_BT	0.0, 0.25, 0.50, 0.75, 1.0, 1.5, 2.0
s [Å]	5.0, 12.5, 25.0, 37.5, 50.0, 55.0, 67.5, 75.0, 125.0, 200.0, 300.0

For the reference and 1 node systems, radial distribution functions, $g(r)$, between the polymer chain and NP were calculated. In addition, probabilities for the end-to-end distance, r_{ee}, and radius of gyration, r_g, were calculated for these systems according to Equations 2.11 and 2.10. These values were used to see if there was a significant effect on the polymer chain being stuck at one end, or if it would behave as a loose polymer in solution.

For all chain systems, loops, tails and trains statistics were considered. In addition, adsorption statistics for chains and segments along the polymer as well as chain-bead contact probabilities, were analyzed.

The polymer network consisted of 88 chains and 35 tetra-functional crosslinks or nodes. These were set in a diamond lattice structure, with both loose dangling chains on the surface, which were only connected to one node at one end, and inner chains connected to nodes at both ends. The initial configuration of the polymer network together with the NP can be seen in Figure 3.3.

For the polymer network system, the radius of the NP was 40.0 Å,

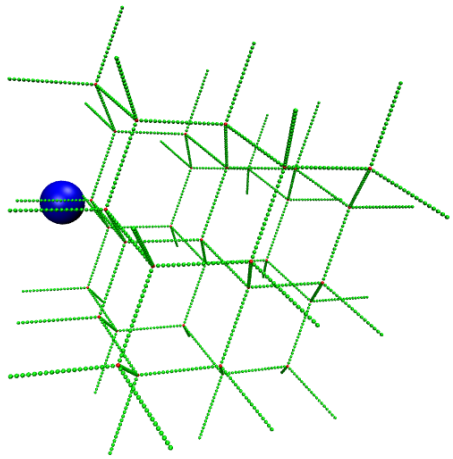

Figure 3.3: Snapshots from the initial configuration of the polymer network. Polymer segments are colored green and network-restricted nodes are red. The nanoparticle is depicted as blue.

the LJ parameter $\sigma = 49.84\,\text{Å}$ and the contact radius $r_{\text{contact}} = 56.57$ approximately corresponding to the ratio $r_{\text{contact}}/r_{\text{min}} = 1.03$. Interaction strengths ε/k_BT equal to 0.0 and 1.0 were investigated for varying force constants, k_{ang}, of the angle potential force. The values evaluated were $k_{\text{ang}} = 0.000,\ 0.002,\ 0.006,\ 0.010$ and $1.000\,\text{kJ}\,\text{mol}^{-1}$, respectively. Increasing the stiffness of the chains is equivalent to increasing swelling in the gel.

The radius of gyration and chain-bead contact probabilities for the systems were calculated. For the contact probabilities, the values were given as either a normalization over all all chains in the system or as a normalization over only the chains of the polymer network interacting with the NP.

Chapter 4

Results and discussion

This chapter is organized so that results pertaining to the NP adsorption to restricted polymer chains are presented first. Then the initial results of the look at adsorption of a single NP to a polymer network are presented.

Figure 4.1 shows snapshots of the 2 node system. The snapshots are taken from simulations with $\varepsilon/k_BT = 1.0$. The node separation, s, increases from 0 through 50, 125, 200 to 300 Å for figures 4.1(a) through 4.1(e), respectively. Similarly, Figure 4.2 shows snapshots of the polymer network for increasing angle potential, k_{ang}. These snapshots are taken from simulations with $\varepsilon/k_BT = 1.0$, and k_{ang} equal to 0.000, 0.002, 0.006, 0.010 and 1.000 kJ mol^{-1}. Figure 4.3 shows the polymer gel system for $\varepsilon/k_BT = 0.0$, for k_{ang} equal to 0.000 kJ mol^{-1} (a) and 0.010 kJ mol^{-1} (b). Values for the force constant of the angle potential between these will yield an intermediary of these figures, and for higher values the system will look more like that of the initial conformation shown in Figure 3.3. Note that these snapshots are only added to give a deeper understanding of the system configuration, but are not to be considered in a quantitative manner.

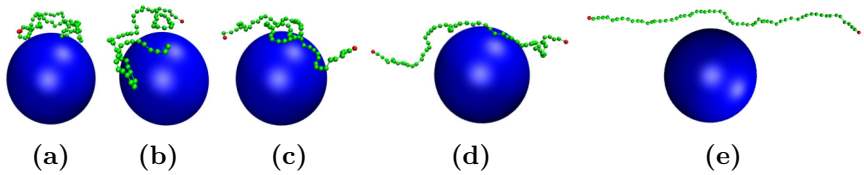

Figure 4.1: Snapshots of the interaction between the polymer chain with two nodes and nanoparticle at $\varepsilon/k_BT = 1.0$ for increasing node separation s (0, 50, 125, 200 and 300 Å for (a) through (e), respectively). Nodes are colored red, while monomers that are allowed to move during the simulation are colored green. The nanoparticle is depicted as blue.

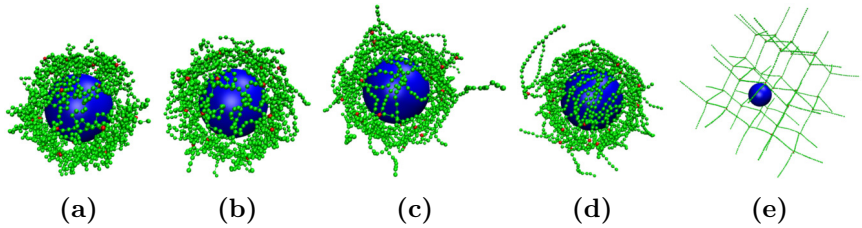

Figure 4.2: Snapshots of the interaction between the polymer network and nanoparticle at $\varepsilon/k_BT = 1.0$ for increasing force constant of the angle potential, k_{ang} (0.000, 0.002, 0.006, 0.010 and 1.000 kJ mol^{-1} for (a) through (e), respectively). Polymer segments are colored green and network-restricted nodes are red. The nanoparticle is depicted as blue.

4.1 Polymer distribution functions

To study the effects of a fixed end monomer on the interaction between a polymer and NP in comparison to a fully free chain, a comparison of the chain statistics of different distribution functions and radii has been made. These properties are only compared between the 1 node and reference systems, as they are not applicable in the systems with a higher number of nodes.

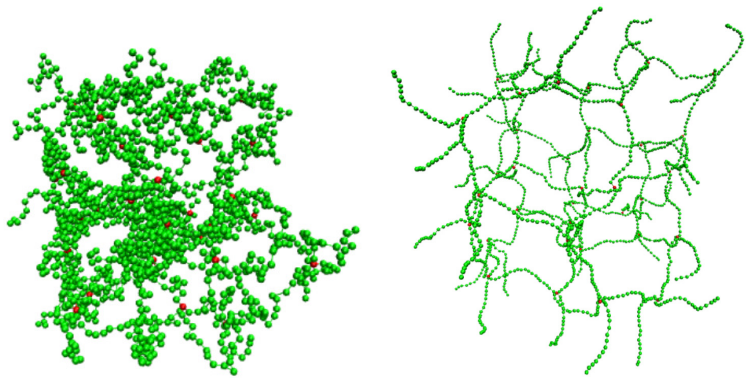

(a) **(b)**

Figure 4.3: Figures (a) and (b) shows snapshots of the polymer network for $k_{\text{ang}} = 0.00\,\text{kJ}\,\text{mol}^{-1}$ (a) and $k_{\text{ang}} = 0.10\,\text{kJ}\,\text{mol}^{-1}$ (b) at $\varepsilon/k_BT = 0.0$. Nodes are colored red, chain beads are colored green and the nanoparticle is blue.

Figures 4.4, 4.5 and 4.6 show the radial distribution function $g(r)$, the probability for the end to end radius, $P(r_{ee})$, and the probability for the radius of gyration, $P(r_g)$, for increasing potential ε/k_BT. The panels denote the 1 node system (a) and the reference system (b), respectively.

For the radial distribution functions, there is little visible difference between the 1 node and reference systems, as seen in Figure 4.4. For both systems, a maximum is obtained at a radial distance, r, that corresponds to the minimum of the LJ potential, r_{min}. In addition, the stronger the potential is, the more likely it is to find the chain monomers adsorbed close to the NP surface. This can be seen in the increase in height of the peak and decrease in width for $\varepsilon/k_BT = 0.25$ (dashed orange line) compared to $\varepsilon/k_BT = 2.00$ (dash-dotted light purple line) in Figure 4.4. As expected, as the potential increases, the chain will adsorb increasingly to the NP, and a highetr number of segments of the chain will be in the

maximum of the potential well, at $r_{\min} = 67.3\,\text{Å}$. For all potentials there is an abrupt decrease at approximately 61.7 Å, corresponding to σ where the LJ potential is highly repulsive. The width of the peak is large, which may indicate that the chain has some degree of freedom to move along either side of the minimum of the potential.

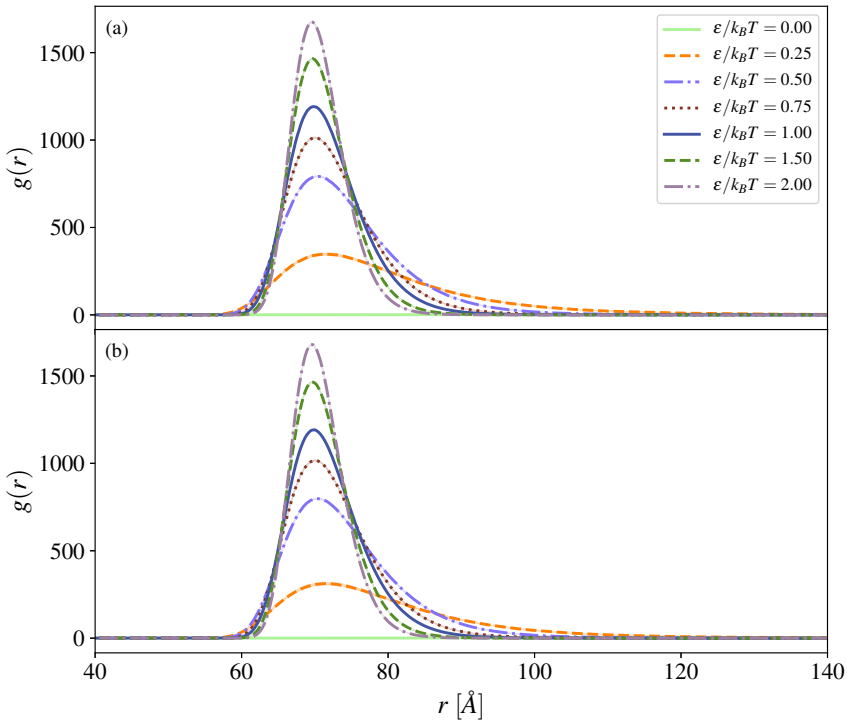

Figure 4.4: Radial distribution function, $g(r)$, for the 1 node (a) and reference (b) systems for different ε/k_BT between the monomers in the polymer chain and the nanoparticle. Legends are shared between columns and the error (standard deviation) is included as a shadow in the same color as the corresponding line.

For the end-to-end radius, r_{ee}, (Figure 4.5) there is a slight difference between the 1 node and reference systems. To interpret the variations of r_{ee}, one can suggest that two effects are occuring.

The first effect is how the polymer adsorbs to the NP in two steps for increasing potential. As the NP and polymer begin to interact, the end-to-end distance first decreasing as the polymer adsorbs to the NP. After the initial decrease, as the potential increases, the polymer adsorbs more strongly to the NP, resulting in the polymer stretching across the surface of the NP, causing an increase in end-to-end radius. In Figure 4.5, this can be seen as a decrease in the end-to-end radius for the polymer from $\varepsilon/k_BT = 0.0$ (green solid line) to $\varepsilon/k_BT = 0.75$ (dark red dotted line) for both the 1 node and reference systems, and ε/k_BT increases, r_{ee} increases until it reaches a maximum for $\varepsilon/k_BT = 2.0$ (light purple dash-dotted line).

The second effect is seen in Figure 4.5(a) for the 1 node system at $\varepsilon/k_BT = 0.25$ (orange dashed line), as a bimodal distribution for the $P(r_{ee})$. This may indicate that the system is in one of two conformations, either adsorbed to the NP or free. As the potential increases, the changes follows those described above. Similar results for the transition between two states have been seen for polymers in high concentrations, but at strong interaction strength, where the polymers seem to be in one of two states depending on whether they are adsorbed to the NP or not (Christiansen 2017).

For the reference system, Figure 4.5(b), there is no bimodal distribution. In this system, the change in conformations seems to appear for lower potentials, and the shift to a larger end-to-end distance can be seen already for $\varepsilon/k_BT = 0.75$ (dark red dotted line). This may suggest that the free polymer adsorbs more readily to the NP than the polymer with one restricted end.

Figure 4.6 shows the $P(r_g)$, where a similar trend as that described for $P(r_{ee})$ is observed. As with the values for the end-to-end distance, r_g

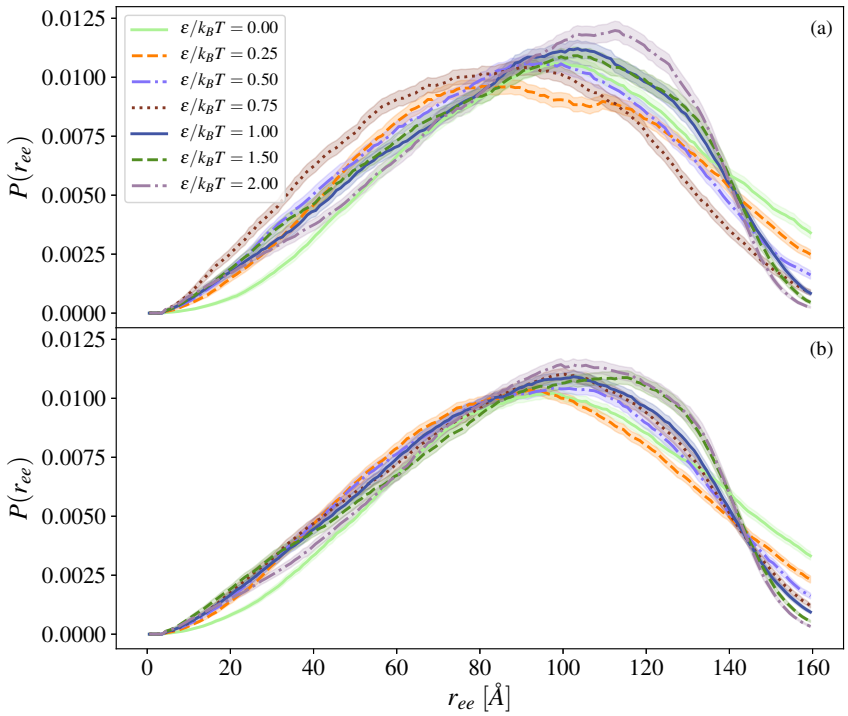

Figure 4.5: Probability for the end-to-end radius, $P(r_{ee})$, for the 1 node (a) and reference (b) systems for different potentials, ε/k_BT. Legends are shared between columns and the error (standard deviation) is included as a shadow in the same color as the corresponding line.

decreases before increasing, as the potential increases. Comparing the two systems, Figure 4.6(a) shows that the 1 node system requires a stronger potential interaction to transition to the lower value as $\varepsilon/k_BT = 0.25$ (orange dashed line) has a wider peak. Again, the transitions seem to occur for weaker potentials for the reference system, as seen for $\varepsilon/k_BT = 0.25$ (orange dashed line) in Figure 4.6(b).

Though the radial distribution functions show no significant differences between the reference and 1 node systems, there seems to be some small differences between the probability of interactions for weak potentials. The

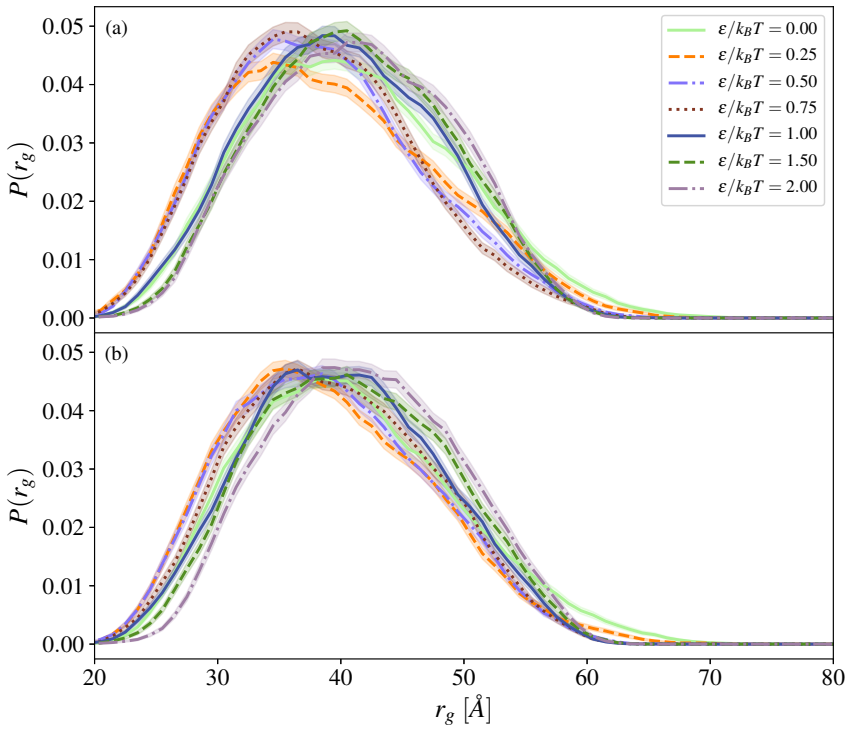

Figure 4.6: Probability for the radius of gyration, $P(r_g)$, for the 1 node (a) and reference (b) systems for different potentials ε/k_BT. Legends are shared between columns and the error (standard deviation) is included as a shadow in the same color as the corresponding line.

end-to-end distance and radius of gyration suggest a distribution between adsorbed and non-adsorbed conformations for these low potentials. This is seen in Figure 4.5(a) as a bimodal distribution and a wider peak for the radius of gyration in Figure 4.6 at $\varepsilon/k_BT = 0.25$, and was also observed when inspecting the snapshots. In the corresponding distributions for the reference system, this is not observed. This suggest that the free chain adsorbs more readily to the NP at lower potentials.

4.2 Adsorbed polymer chains and segments

Figures 4.7, 4.8 and 4.9 show the average number of adsorbed chains $\langle N_{\text{ads\_ch}} \rangle$ and segments $\langle N_{\text{ads\_seg}} \rangle$, for the 1 node and reference systems, 2 node and 3 node system, respectively.

For the 1 node and reference systems, the number of adsorbed chains and segments increases at a similar pace when increasing the attractive potential (Figure 4.7). Regarding the number of adsorbed chains, Figure 4.7(a) shows a slightly lower probability of the chain adsorbing to the polymer for $\varepsilon/k_BT = 0.25$ for the 1 node system (green solid line) than that of the reference system (orange dashed line) at the same potential. This is in agreement with the indication that there is a possibility of the chain being either adsorbed or non-adsorbed to a larger extent for the 1 node system than for the reference system when evaluating the probability distributions $P(r_{ee})$ and $P(r_g)$.

For the number of adsorbed segments there seems to be a higher probability for the reference system to interact randomly with the NP than the 1 node system. There is also a significantly larger error (standard deviation) for the reference system at zero potential, as would be expected. As the attractive potential increases, the interactions are similar, and the average number of adsorbed segments increase from 10 monomers at $\varepsilon/k_BT = 0.25$, to 25 monomers at $\varepsilon/k_BT = 2.00$.

The lower number of adsorbed chains for $\varepsilon/k_BT = 0.25$ is a result of the interacting potential not being able to overcome the loss of entropy for adsorption of the chain to the NP. According to Equation 2.3, the potential must be stronger than $\varepsilon/k_BT = 0.4$ for the polymer to adsorb to a surface. At $\varepsilon/k_BT = 0.25$, the attractive potential may be too weak to for the NP to adsorb completely. The NP-polymer complex fluctuates

between the adsorbed and non-adsorbed state, as the acting potential competes against the effects of the loss of conformational entropy.

It may also be worth noting that the reference system shows a slightly higher chance of interacting with the NP, than the 1 node system. This is inferred by the higher number of adsorbed segments for the non-interacting systems. Again, this difference seems to be insignificant at higher potentials, and the error (standard deviation) for the non-interacting reference system is large.

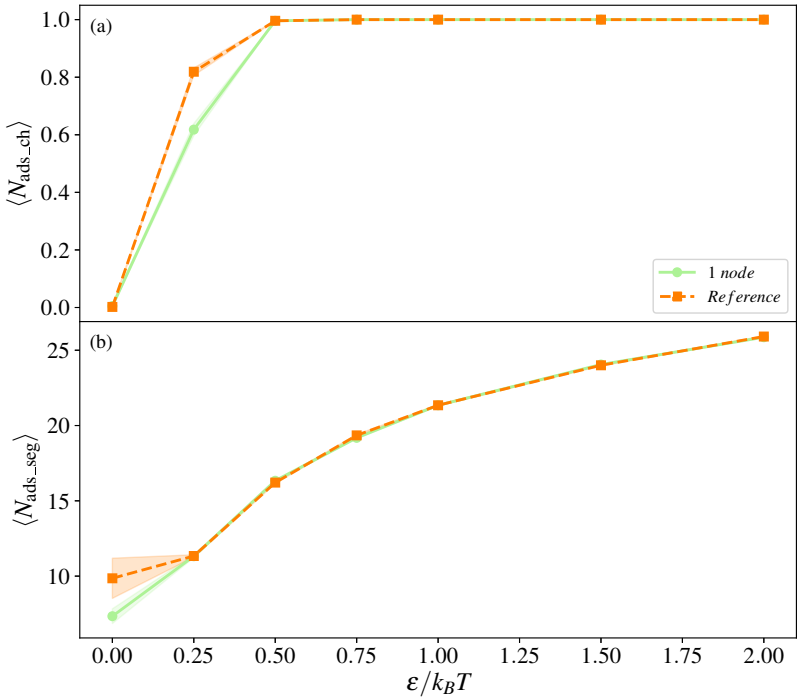

Figure 4.7: Average number of adsorbed chains, $\langle N_{\text{ads\_ch}} \rangle$, and segments, $\langle N_{\text{ads\_seg}} \rangle$, for the 1 node and reference systems. Legends are shared between columns and the error (standard deviation) is included as a shadow in the same color as the corresponding line.

Figure 4.8 shows the average adsorption of chains $\langle N_{\text{ads\_ch}} \rangle$, and segments, $\langle N_{\text{ads\_seg}} \rangle$ as a function of node separation s (panels (a) and (c)), and as a function of the potential energy ε/k_BT (panels (b) and (d)), for the 2 node system. As a function of the potential, Figure 4.8(b) exhibits a lower average for the adsorbed amount of chains for $s = 200.0$ Å (light blue dashed line) and $s = 300.0$ Å (red dash-dotted line) at $\varepsilon/k_BT = 0.25$. For these node separations there is an average chain adsorption of about 0.4 and 0.2 respectively, compared to approximately 0.8 for the shorter node separations. As the potential increases, the chain has full probability of being adsorbed to the NP.

Regarding the adsorption of the chains as a function of s, Figure 4.8(a) indicates that the NP has a maximum probability of adsorbing to the chain for systems with potential greater than $\varepsilon/k_BT = 0.75$. For $\varepsilon/k_BT = 0.25$ (orange dashed line) the number of adsorbed chains fluctuates, and decreases as the node separation increases. When viewing the snapshots, it is clear that the NP adsorbs and desorbs from the chain for different steps, causing the fluctuation of the average adsorbed number of chains for this potential. This effect can also be seen for $\varepsilon/k_BT = 0.50$ (indigo dash-dotted line) and $\varepsilon/k_BT = 0.75$ (dark red dotted line), which are otherwise adsorbed, for $s = 300$ Å in Figure 4.8(a). This is consistent with what was inferred by the 1 node system.

With an increase in the node separation, the number of adsorbed monomers decreases. As a function of ε/k_BT, the opposite is observed when the interacting strength is increased, as can be seen in Figure 4.8, panels (c) and (d). This is in good agreement with the reference and 1 node systems. The effect of increasing ε/k_BT is smaller for the longer node separations (light blue dashed line and red dash-dotted line in Figure 4.8(d)). With an increase in node separation, the number of segments

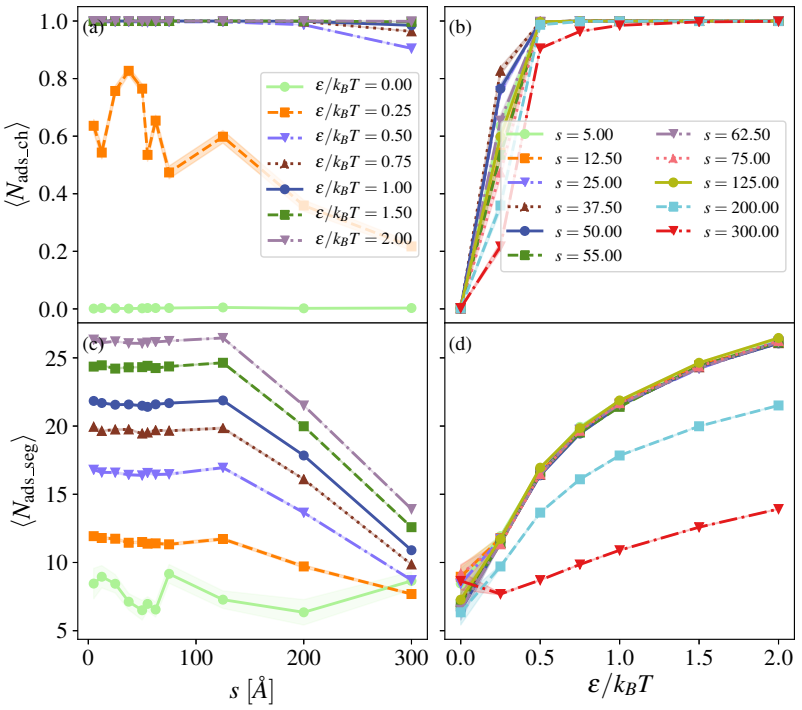

Figure 4.8: Average number of adsorbed chains, $\langle N_{\text{ads\_ch}} \rangle$, and segments, $\langle N_{\text{ads\_seg}} \rangle$, for a polymer chain with two nodes. Panels (a) and (c) show the adsorption as a function of node separation s, and (b) and (d) as a function of potential, ε/k_BT. Legends are shared between columns and the error (standard deviation) is included as a shadow in the same color as the corresponding line.

that can interact with the NP decreases as a result of the restriction to the chain from the nodes. The monomers in the polymer chain will not be able to wrap around the NP, as in the 1 node and reference systems, resulting in an overall decrease in number of adsorbed segments and chains.

Figure 4.9 shows the adsorption of chains $\langle N_{\text{ads\_ch}} \rangle$, and segments, $\langle N_{\text{ads\_seg}} \rangle$ as a function of node separation (panels (a) and (c)) and as a function of the potential energy (panels (b) and (d)) for the 3 node system. As seen in the 2 node system, when a potential of $\varepsilon/k_BT = 0.25$ is applied

the NP adsorbs more weakly to the polymer. For the 3 nodes system the effect of adsorption reduction with increasing s is clearly seen in Figure 4.9(a). For $\varepsilon/k_BT = 0.25$ (orange dashed line) when s exceeds 100 Å the probability of adsorption decreases to the point where the NP adsorption is 0.5.

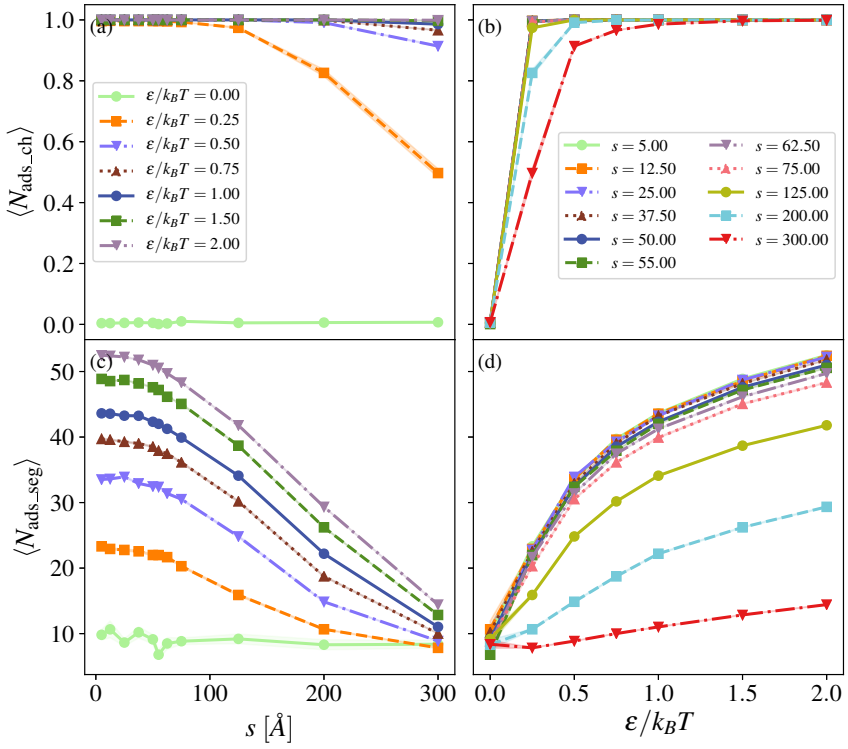

Figure 4.9: Average number of adsorbed chains, $\langle N_{\text{ads\_ch}} \rangle$, and segments, $\langle N_{\text{ads\_seg}} \rangle$, for a polymer chain with three nodes. Panels (a) and (c) show the adsorption as a function of node separation s. (b) and (d) show the adsorption as a function of potential, ε/k_BT. Legends are shared between columns and the error (standard deviation) is included as a shadow in the same color as the corresponding line.

Regarding the average number of adsorbed segments in the 3 node

system, we see that the number of adsorbed segments is twice that of the number of adsorbed segments found for the 2 node system, at low node separations. This can be seen clearly when comparing figures 4.8(c) and 4.9(c), and indicates that the NP is in contact with both polymer chains. For the 3 node system the number of adsorbed segments decreases faster than for the 2 node system, and at $s = 300\,\text{Å}$, the number of adsorbed segments is similar.

In Figure 4.9(d) it is also indicated that the number of adsorbed segments decreases faster for a decreasing potential, compared to the 2 node system. The effect on the number of adsorbed segments for increasing potential, decreases with increasing node separation. At $s = 300\,\text{Å}$ (red dash-dotted line) and an increasing potential is applied, it can be seen that for both the 2 node and 3 node systems, the number of adsorbed segments reaches a maximum of about 14 segments for $\varepsilon/k_BT = 2.00$. This suggests that the NP adsorbs to the polymer in a similar fashion for both the 2 node and 3 node system when the node separation is large.

For all systems there is an increase in number of adsorbed segments and chains for increasing potential. For 2 nodes and 3 nodes, the number of segments decreases with increasing s, as seen in figures 4.8(c) and 4.9(c). This is as expected. As the polymer gets stretched with increasing node separation, the polymer will not be able to wrap around the NP, and fewer monomers along the chain will interact with the NP as the movements of these are restricted by the nodes.

4.3 Loops, tails and trains

Number of loops, tails, and trains in the 1 node and reference systems are shown in Figure 4.10, and the length of these in Figure 4.11. As

the potential increases, the number of trains and loops increases and the number of tails decreases. The length of loops, tails and trains all decrease with increasing potential, indicating an increasing amount of short loops and trains on the surface of the NP. For weak potentials, $\varepsilon/k_BT = 0.25$ the tails are long, but reduce quickly with the increasing potential. The length of the loops are approximately twice that of the trains, consistent with previous findings, demonstrating that polymers will prefer long loops and short trains, as the polymer will prefer to retain as much conformational entropy by having loose segments. This ratio is rapidly reduced, as the length of the loops decreases quickly with an increase of the attractive potential.

To summarize, as the interaction between the NP and monomers increases, the number loops and trains increase and the length of each of these decrease. This shows that the polymer transitions from a conformation consisting of few long loops, and few short trains to many short loops and trains. The tails decrease, showing a to further extent the adsorption to the NP, in good agreement with Figure 4.7.

Again, the reference and 1 node systems show very similar results. Large variations are seen only for the non-attractive system, where the NP occasionally gets close to the polymers. The 1 node system with $\varepsilon/k_BT = 0.25$ shows a slightly larger number of loops, but this does not seem to effect the number of adsorbed monomers (Figure 4.7(b)).

Figure 4.12 shows the average number of adsorbed loops, tails and trains for the 2 node system, as a function of s (panels (a), (c) and (e)), and ε/k_BT (panels (b), (d) and (f)). As observed for the 1 node system, the average length of these chains indicators decreases with increasing ε/k_BT. As seen for the average number of tails, trains and loops, systems with larger s deviate from the other results with the length of the indicator

decreasing more slowly with increasing potential. In the case of $\langle l_{\text{loops}} \rangle$, there is even a slight increase with ε/k_BT. If one looks specifically to the tail length, $\langle l_{\text{tails}} \rangle$, the length of the tails is seen to decrease less for longer node separations, when the potential is increased.

The number of loops and trains remains constant with separation until they decrease, as would be expected (Figure 4.12(a) and (c)). In Figure 4.13(d) a decrease in $\langle N_{\text{tails}} \rangle$ for all node separations is observed, suggesting that the NP is more centered for stronger interactions. This in turn reduces the tails even for long node separations.

The left-hand panels in Figure 4.11 describe the evolution of $\langle l_{\text{loops}} \rangle$, $\langle l_{\text{tails}} \rangle$ and $\langle l_{\text{trains}} \rangle$ with increasing separation. One sees that for all the systems, with varying ε/k_BT, the increase in s leads to a decrease in the length of loops and an increase in tails and trains. As one increases s, the system evolves from many long loops, to one slightly longer train, and significantly longer tails, as expected. The longest tail is found for $\varepsilon/k_BT = 0.25$ (orange dashed line) as suggested in Figure 4.11(c), which is consistent with this system having fewer adsorbed monomers (Figure 4.7(d)).

Figure 4.13 shows the average length of the loops, tails and trains for the 2 node system varying with s for panels (a), (c) and (e), and ε/k_BT for panels (b), (d) and (f). Figure 4.13(d) shows a decrease in the tail length for all node seperations, suggesting that the NP pulls more at the chain for stronger interactions, which reduces the length of tails slightly even for long node separations. The orange dashed line in Figure 4.13(c) suggests that the tails are longest for $\varepsilon/k_BT = 0.25$. The length of the loops decreases with increasing potential (Figure 4.13(a)), while the length of the tails and trains increases (Figure 4.13(c) and (e)). This is opposite of what happened with the 1 node system, and is likely an effect of the

chain being stretched and is restrained in it's formation of loops.

The average number of loops, tails and trains for the 3 node system are found in Figure 4.15 as a function of the node separation s and a function of the potential ε/k_BT. For increasing ε/k_BT, the number of loops and trains increases, as the polymer chains wrap closer to the NP. This effect is similar to the 1 node and 2 node systems for small node separations. As the node separation increases, the effect of increasing the potential is reduced, and for $s = 300\,\text{Å}$ (red dash-dotted line), there almost no increase, as shown in the right-hand side of Figure 4.15.

With increasing attractive potential, Figure 4.15(d) shows that the length of the tails is highly dependent on the node separation. As the potential increases the number of tails increases to the limit of 2 tails for node separations larger than 37.5 Å. In Figure 4.15 for $s = 37.5\,\text{Å}$ (dark red dotted line) we see that the number of tails fluctuates at a value sightly higher than 1.6, and for smaller node separations the number of tails decreases with the increasing potential. At approximately $s = 30\,\text{Å}$ the NP will still be able to interact with all three nodes, but as the separation increases it will not be able to interact with more than two. This is an effect of the nodes being fixed in the system, and the separation being too large for the polymer to adsorb close enough to all three nodes at the same time due to the strong repulsion for the LJ potential at values lower than σ. Instead of adsorbing to either node pair, middle and first, or middle and last node, the NP seems to prefer to stick to the center node of the polymer chain. Here the NP can wrap closely to the residual chains from either side, and maximize the number of interacting monomers.

The number of tails varies more abruptly, from $\langle N_{\text{tails}} \rangle = 1.2$ to 2.0, for increasing potential, achieving the maximum value at approximately $s = 50\,\text{Å}$. An increase in ε/k_BT also leads to a larger $\langle N_{\text{tail}} \rangle$ (Figure

4.15(d)) when compared to the 2 node system. This is likely a consequence of considering the system as one chain. If the polymer adsorbs to the NP close to the central node, it will depict a two tail system, while if the two chain parts of the polymer would have been considered as two chains, bound by a node, a one-tail system would probably arise.

Figure 4.14 shows the average length of loops, tails and trains for the 3 node system as a function of the node separation s (panels (a), (c) and (e)), and ε/k_BT (panels (b), (d) and (f)). The overall trend in Figure 4.14 is the same as those described for the 2 node system, but the system is more sensitive to variations of ε/k_BT, even for short separations s.

As a function of the potential, the length of the loops decrease with increasing potential, suggesting that the polymer forms an increasing amount of short trains and loops, in agreement with the 1 node system. The change in length of trains, as seen in Figure 4.14 is less than 2 Å as the potential increases from $\varepsilon/k_BT = 0.25$ to $\varepsilon/k_BT = 2.0$. On the other hand, the reduction of the tail length is over 40 Å for short node separations. For node separations $s = 200$ Å (light blue dashed line) and $s = 300$ Å (red dash-dotted line), seen in panels (b) and (d) of Figure 4.14, the effect of the increasing potential is small. When the node separation is large, there are less loops forming, and the length of these are short.

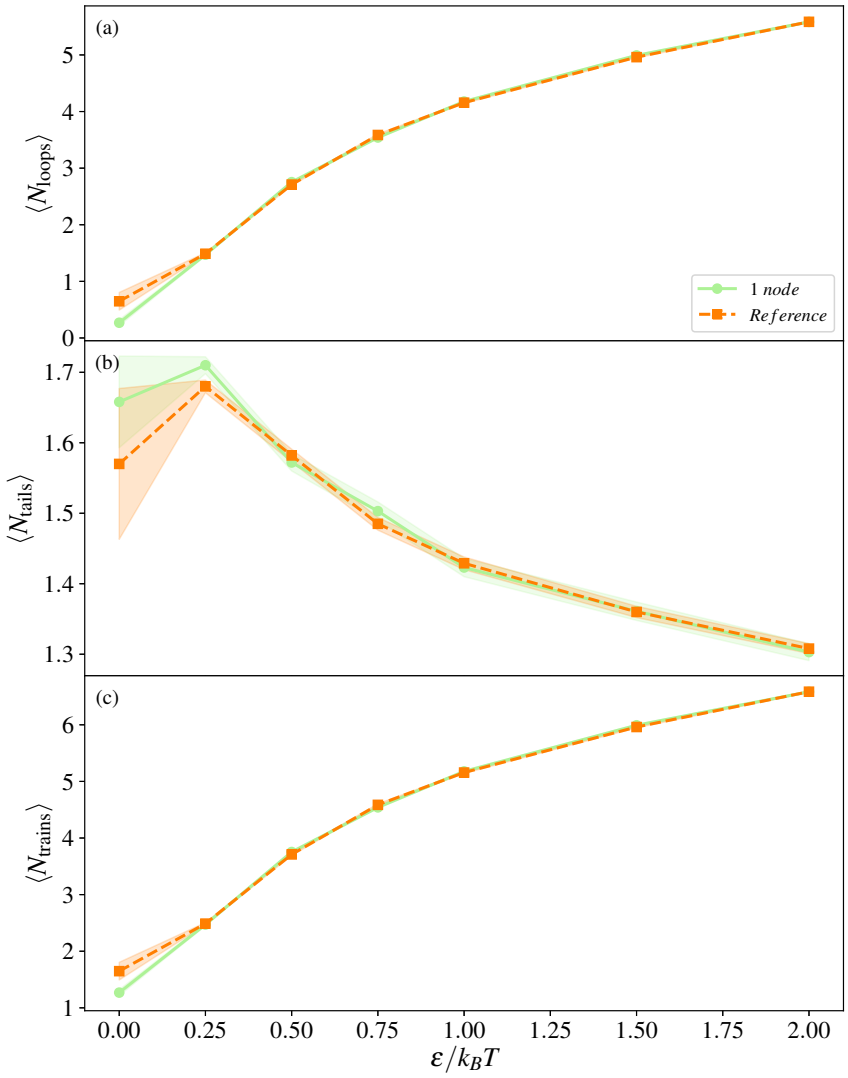

Figure 4.10: Average number, $\langle N_\alpha \rangle$, of loops, tails and trains for system 1 and the reference system as a function of the potential, ε/k_BT. Here α denotes loops, tails and trains respectively. Legends are shared between columns and the error (standard deviation) is included as a shadow in the same color as the corresponding line.

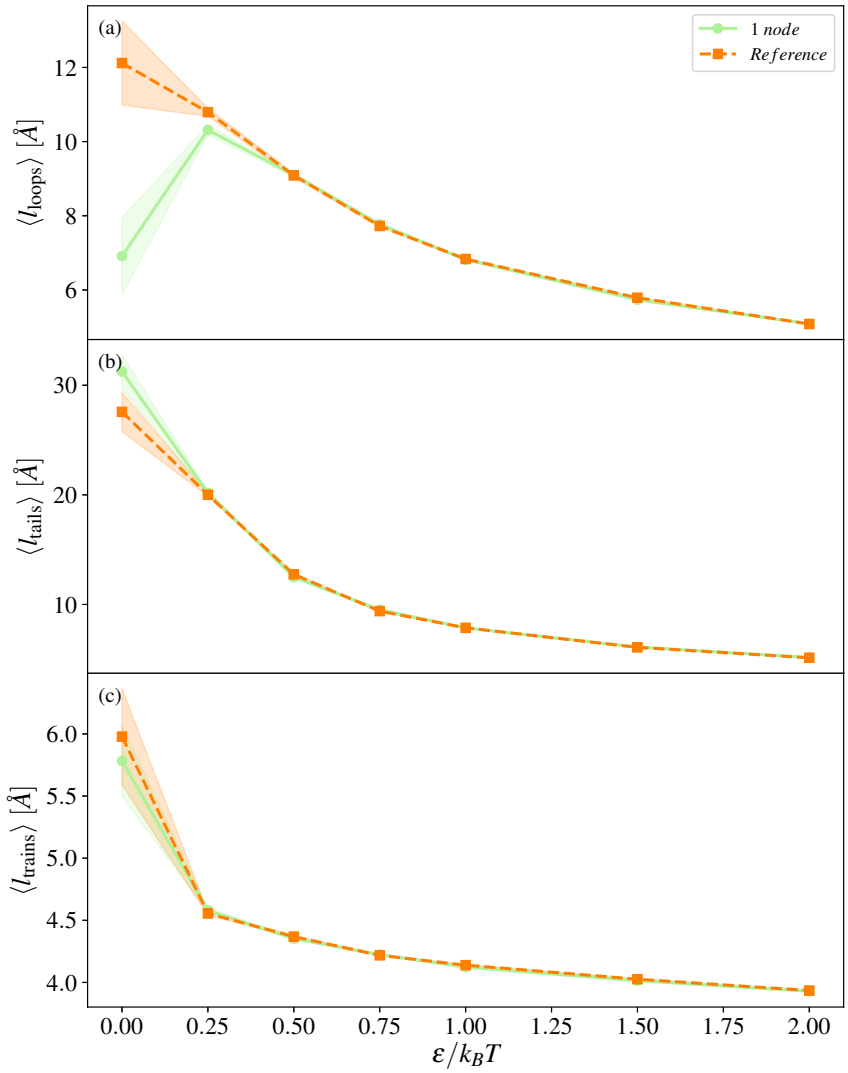

Figure 4.11: Average length, $\langle l_\alpha \rangle$, of loops, tails and trains for system 1 and the reference system as a function of the potential, ε/k_BT. Here α denotes loops, tails and trains respectively. Legends are shared between columns and the error (standard deviation) is included as a shadow in the same color as the corresponding line.

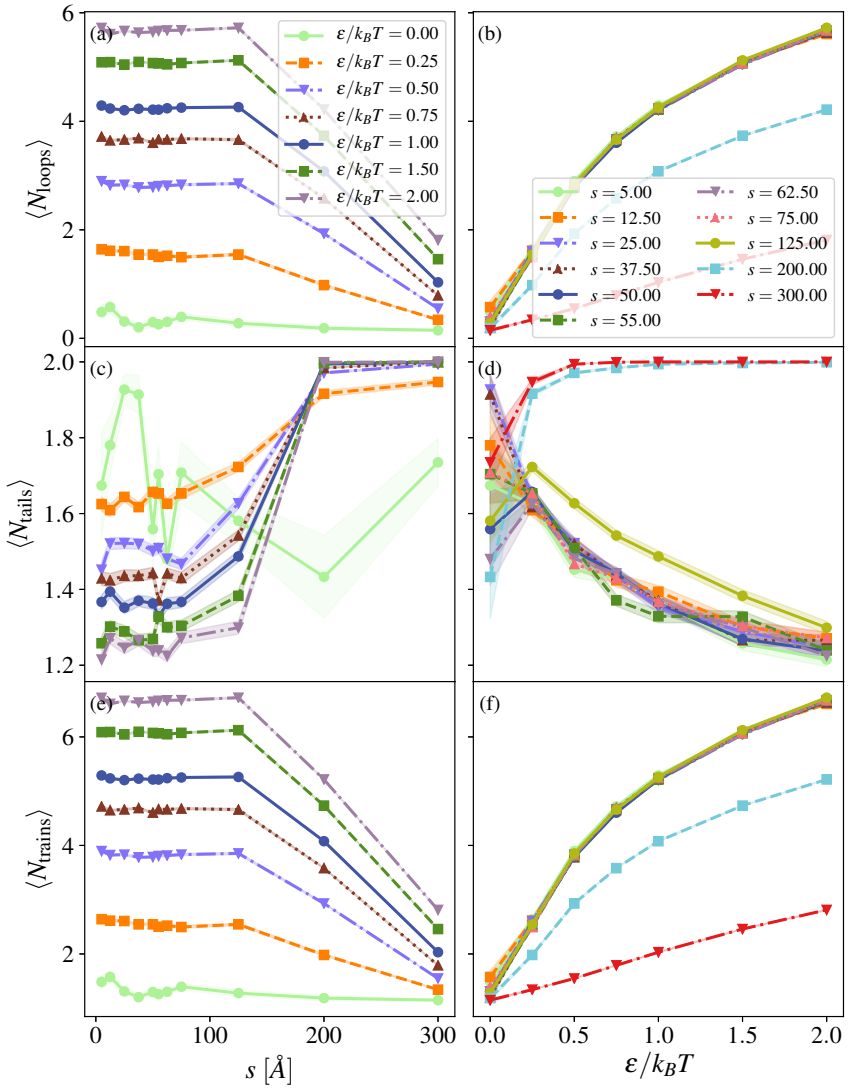

Figure 4.12: Average number, $\langle N_\alpha \rangle$, of loops, tails and trains for system 2. α denotes loops, tails and trains respectively. Panels (a), (c) and (e) show loops, tails and trains as a function of node separation, s. (b), (d) and (f) show loops, tails and trains as a function of the potential, ε/k_BT. Legends are shared between columns and the error (standard deviation) is included as a shadow in the same color as the corresponding line.

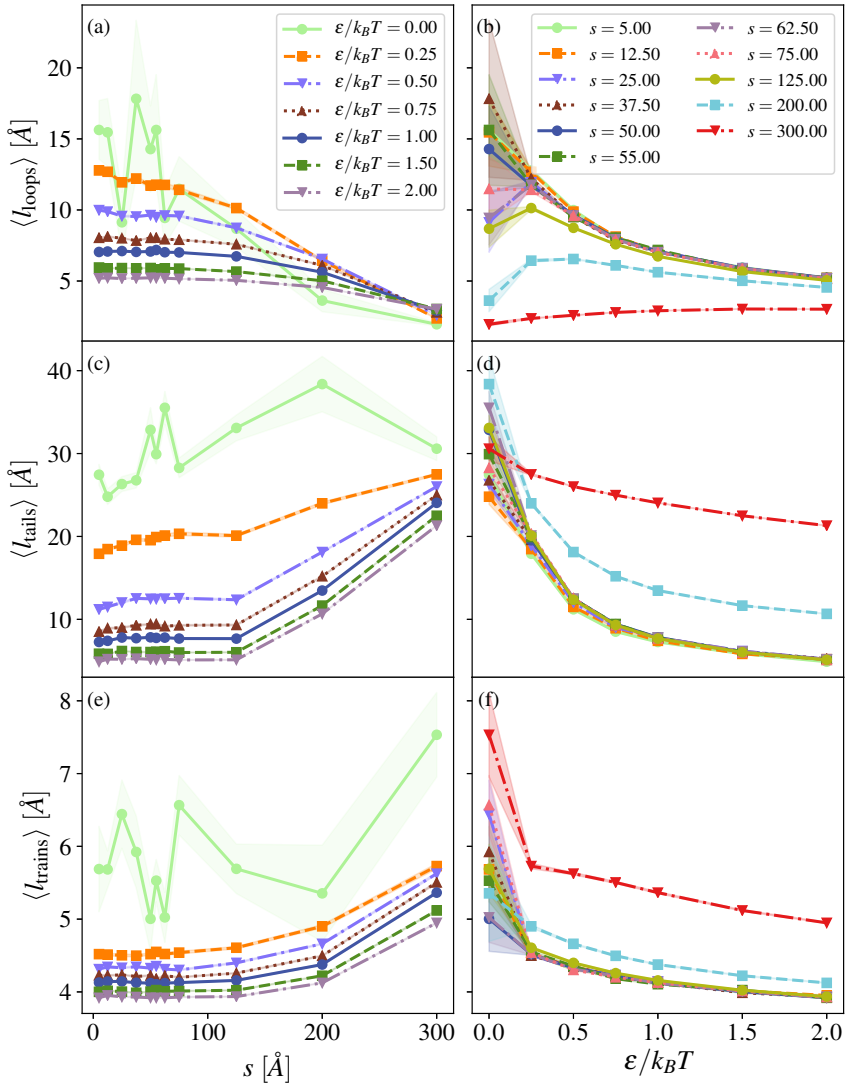

Figure 4.13: Average length, $\langle l_\alpha \rangle$, of loops, tails and trains for system 2. Panels (a), (c) and (e) show loops, tails and trains as a function of node separation, s. (b), (d) and (f) show loops, tails and trains as a function the potential, ε/k_BT. α denotes loops, tails and trains respectively. Legends are shared between columns and the error (standard deviation) is included as a shadow in the same color as the corresponding line.

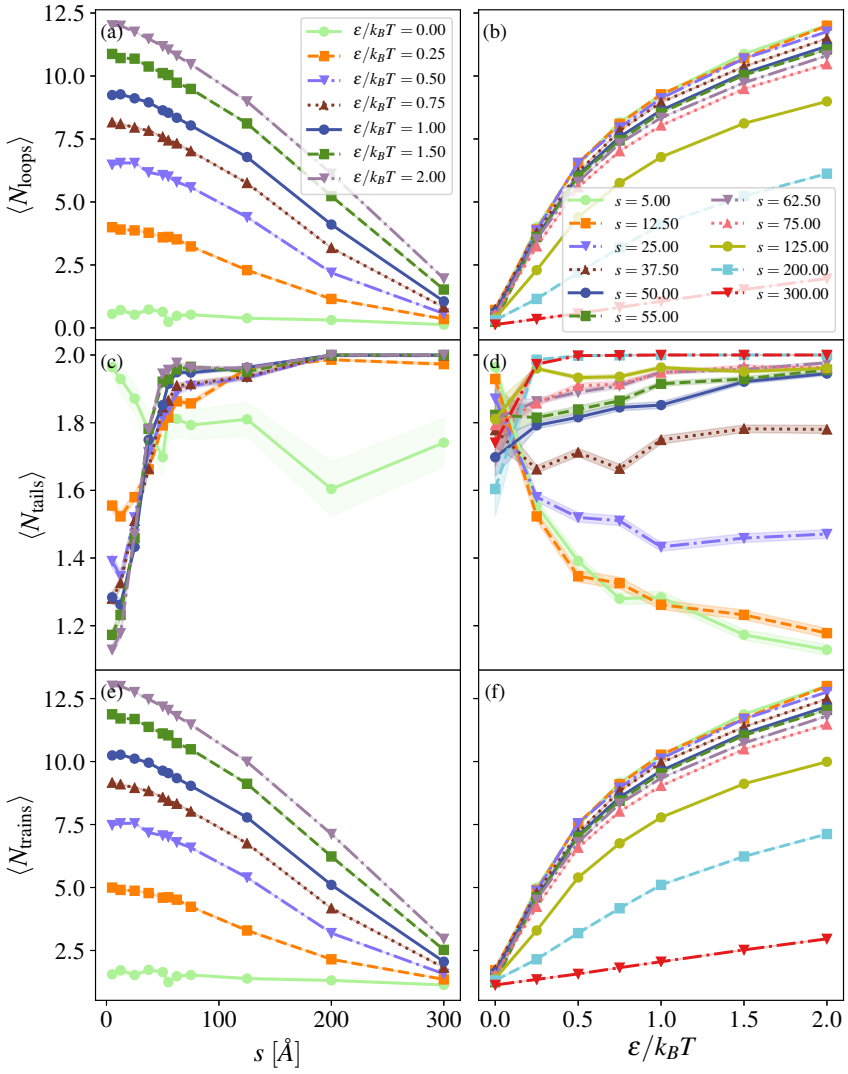

Figure 4.14: Average number, $\langle N_\alpha \rangle$, of loops, tails and trains for system 3. α denotes loops, tails and trains respectively. Panels (a), (c) and (e) show loops, tails and trains as a function of node separation, s. (b), (d) and (f) show loops, tails and trains as a function the potential, ε/k_BT. Legends are shared between columns and the error (standard deviation) is included as a shadow in the same color as the corresponding line.

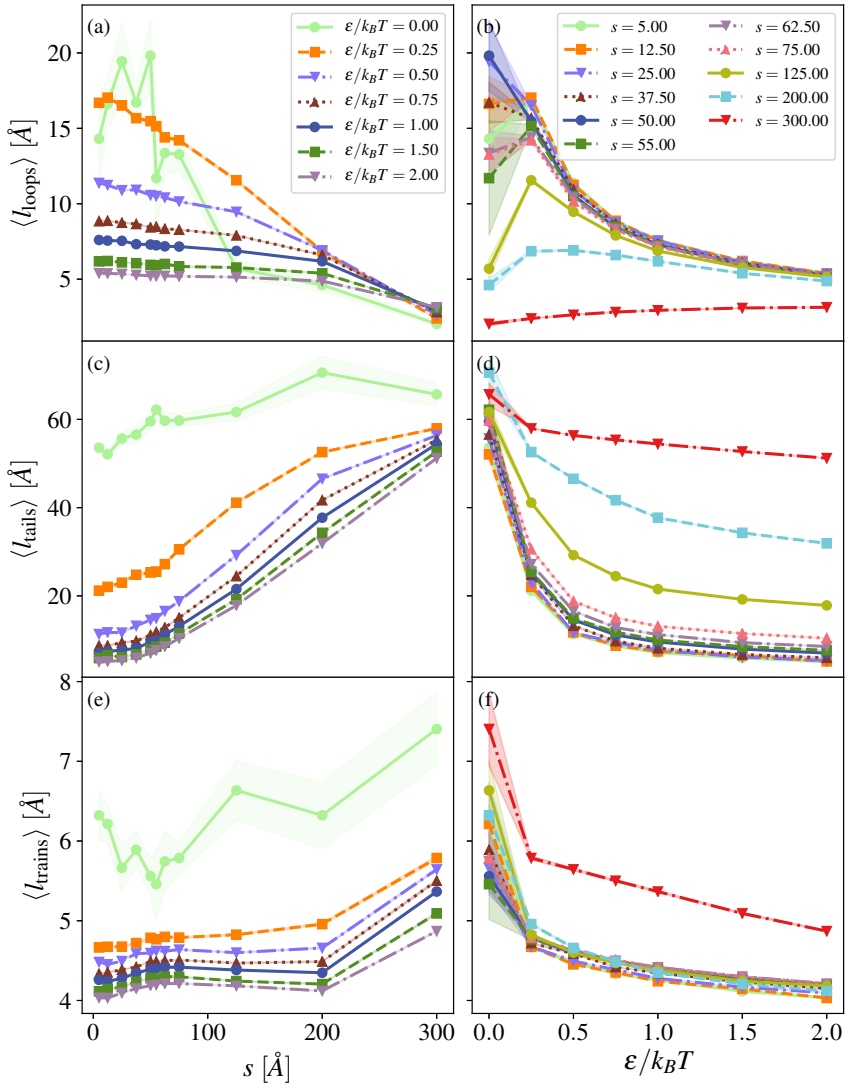

Figure 4.15: Average length, $\langle l_\alpha \rangle$, of loops, tails and trains for system 3. Panels (a), (c) and (e) show loops, tails and trains as a function of node separation, s. (b), (d) and (f) show loops, tails and trains as a function the potential, ε/k_BT. α denotes loops, tails and trains respectively. Legends are shared between columns and the error (standard deviation) is included as a shadow in the same color as the corresponding lines.

4.4 Contact probabilities

The following section presents the probability of finding the NP along the polymer chain, represented by NP-monomer contact probabilities. The monomers are indexed according to their position along the chain, and all chain segments (chains and nodes) are counted as one long chain.

For the 1 node and reference systems, seen in Figure 4.16 (panels (a) and (b) respectively), there is little visible difference between the two systems. As would be expected, the probability of finding a monomer in contact with the NP increases with increasing ε/k_BT, in agreement with Figure 4.7(d). For both systems there is a slight increase in the probability of the node adsorbing to a monomer 7 segments from the ends, suggesting the preferred state is that of one long and one short tail.

Note how the probability of contact, $P(d \leq r_{\text{contact}})$, increases slightly for the first and last monomer along the chain. This increase in the probability decreases as the strength of the potential well increases, and the effect is possibly due to the monomers being capable of fluctuating in the potential well.

Figure 4.17 shows the contact probability for node separations s =5, 50, 125, 200 and 300 Å (panels (a) through (e), correspondingly). As the node separation increases, the probability for the NP to adsorb to the ends tends to zero, and increases for the center monomers of the chain. This decrease in probability at the first and last monomers along a chain is visible for $s = 125$ Å in Figure 4.17 (c). This distance corresponds to the distance of the LJ parameter σ. At this distance the NP will still be able to interacting closely with both nodes and the chain will wrap around the NP.

As the node separation increases beyond this threshold, the probability

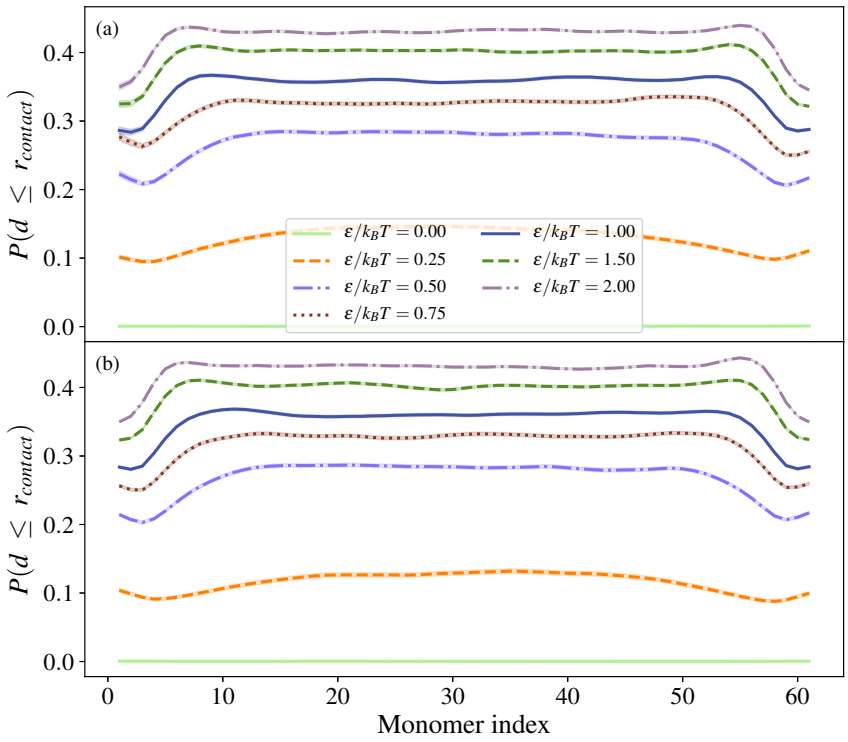

Figure 4.16: NP-monomer contact probability, $P(d \leq r_{\text{contact}})$, of a given monomer for a polymer chain with one node (a) and a free polymer chain (b). Legends are shared between columns and the error (standard deviation) is included as a shadow in the same color as the corresponding line.

of the NP adsorbing to an end decreases to zero, as seen Figure 4.17 (d), in agreement with the number of tails increasing to two as seen in Figure 4.12(c). For $s = 200\,\text{Å}$, there is a slight increase in probability of finding of the NP at a monomer index of 10 from either end for $\varepsilon/k_BT = 2.0$ (light purple dash-dotted line), similarly to the results seen for the 1 node and reference systems, and again indicate the preference for one long and one short tail.

When s increases to 300 Å, Figure 4.17(e) shows that the probability

tends to a Gaussian curve centered on the middle of the chain. For this node separation the overall probability of finding an adsorbed monomer decreases, in agreement with Figure 4.8(c).

The probability of the NP to adsorb to all monomers monomers decreases as the node separation increases for $\varepsilon/k_BT = 0.25$ (orange dashed line), in agreement with the results found for the average chain adsorption (Figure 4.8(a)).

The contact probabilities for all node separations for $\varepsilon/k_BT = 1.0$ and $\varepsilon/k_BT = 2.0$ can be seen in Figure A.4 in appendix A.

The contact probability for the 3 node system is given in Figure 4.18 for s = 5, 50, 125, 200 and 300 Å for panels (a) through (e). At small node separations the NP displays an increase in adsorption potential near the center of the chains. The NP seems to prefer to adsorb close to, but not at the center. The decreasing probability of adsorption at the central node may be a steric effect from hard sphere overlap, as the system is crowded near the nodes. The probability for finding the NP at either end for $s = 5$ Å seems to be larger for the first or last monomer, and smaller for the opposing end. This effect is especially clear for $\varepsilon/k_BT = 1.0$ (blue solid line), where the probability of finding the NP adsorbed to the first particle is almost twice that of finding it at the last monomer. For $\varepsilon/k_BT = 1.50$ (olive dashed line) and $\varepsilon/k_BT = 2.00$ (light purple dash-dotted line) the NP adsorbs to one side of the central node, which leads to the asymmetric cuve in Figure 4.18(a).

As the node separation increases the NP adsorbs more readily to the central node, as seen in Figure 4.18(b). At separations larger than approximately 30 Å, the NP cannot be in contact with more than at the most two of the nodes. The NP prefers the center node, and this is likely due to this being the position along the chain where it can interact with the

maximum number of monomers in a given chain. For the outer nodes the contact probability decreases towards zero.

With further increasing separations of the nodes, the contact probability tends to that seen in the 2 node system. This is seen clearly in Figure 4.18(d), with $s = 200\,\text{Å}$, the contact probability widens and creates a plateau similar to that found for the same node separation in the 2 node system (Figure 4.17(d)). When s increases to $300\,\text{Å}$, the NP prefers one side and sticks to this. This results in a large asymmetry in the contact probability (light purple dash-dotted line and olive dashed line in Figure 4.18(e).

The contact probabilities for all node seperations for $\varepsilon/k_BT = 1.0$ and $\varepsilon/k_BT = 2.0$ can be seen in Figure A.5 in appendix A.

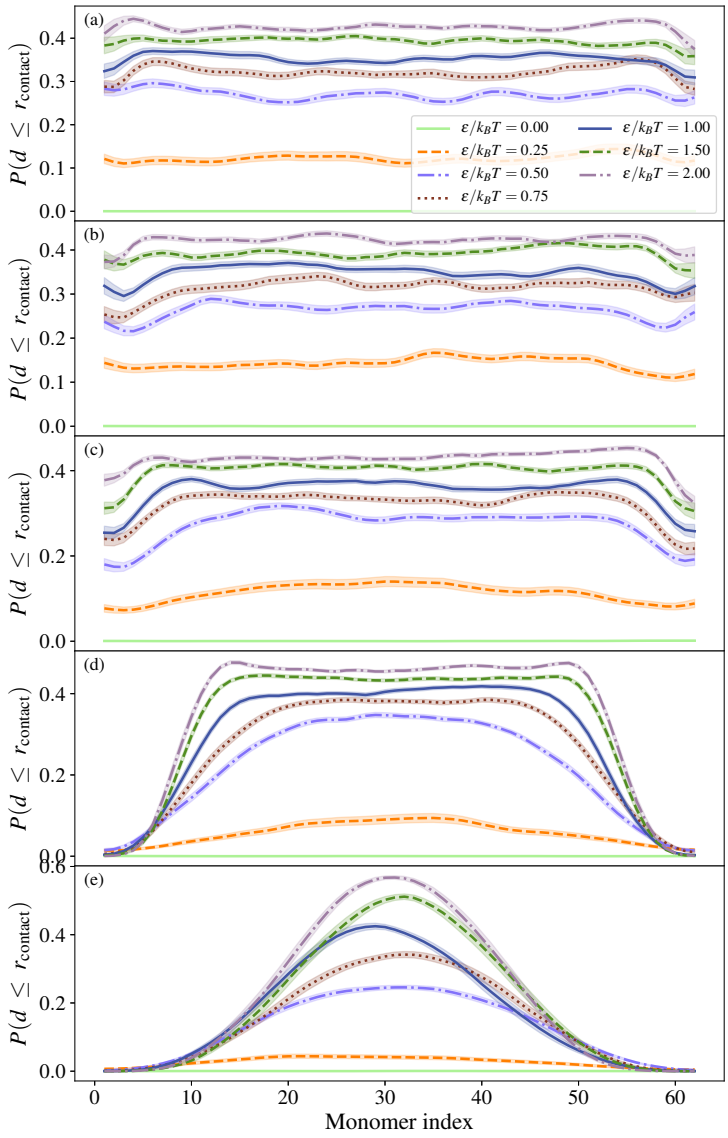

Figure 4.17: NP-monomer contact probability, $P(d \leq r_{\text{contact}})$, of given monomer for 2 nodes. Panels (a) through (e) show the contact probability of a given monomer for increasing node separation s (5, 50, 125, 200 and 300 Å, respectively). Legends are shared between columns and the error (standard deviation) is included as a shadow in the same color as the corresponding line.

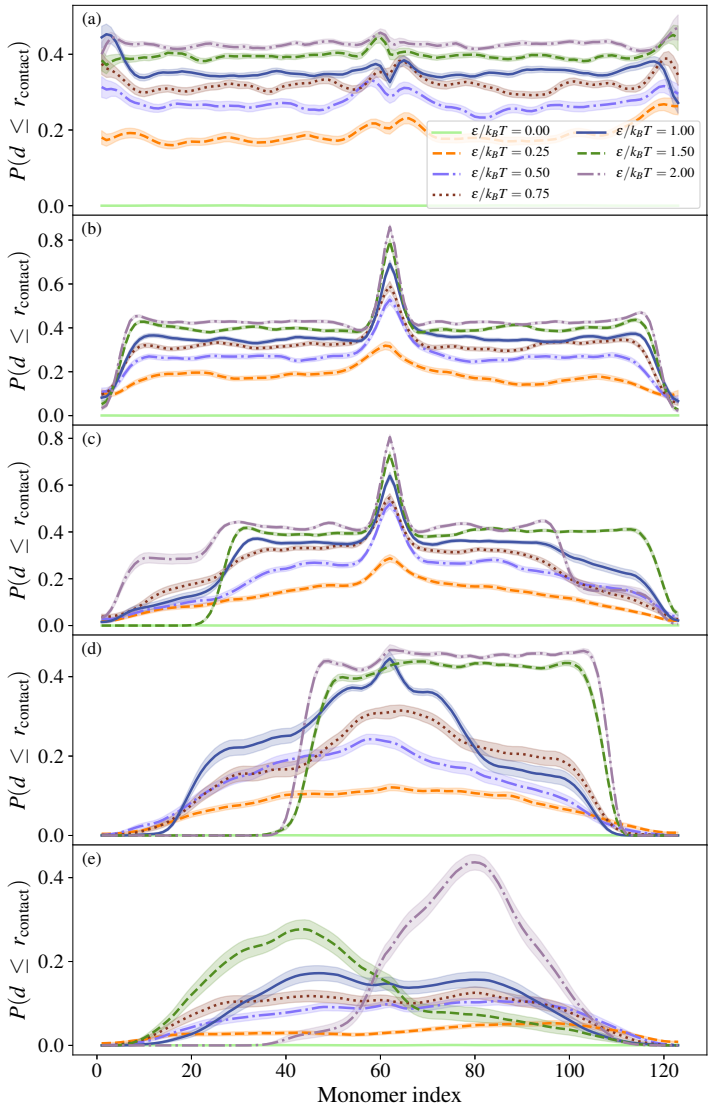

Figure 4.18: NP-monomer contact probability, $P(d \leq r_{\text{contact}})$, of given monomer for 3 nodes. panels (a) through (e) shows shows the contact probability of a given monomer for increasing node separation s (5, 50, 125, 200 and 300 Å, respectively). Legends are shared between columns and the error (standard deviation) is included as a shadow in the same color as the corresponding line.

4.5 Polymer network

Figure 4.19 shows the probability of the radius of gyration, $P(r_g)$, for $\varepsilon/k_BT = 0.0$ in 4.19(a) and $\varepsilon/k_BT = 1.0$ in 4.19(B). The results for $k_{\text{ang}} = 1.0\,\text{kJ mol}^{-1}$ are excluded from the figure, to increase focus on the lower values of the angle potential. For $k_{\text{ang}} = 1.0\,\text{kJ mol}^{-1}$, r_g retained a value of 200 Å before and after the production run.

Figure 4.19(a) shows that as k_{ang} decreases, the r_g decreases. The initial radius of the gel is approximately 200 Å. Maximum packing for the non-interacting polymer network is given by $k_{\text{ang}} = 0.0\,\text{kJ mol}^{-1}$ (red solid line) in Figure 4.20(a), and has a peak just below 70 Å. For low values of k_{ang}, the system collapses, and r_g reduces to a value similar to that of the LJ parameter σ. The slightly larger value may be because of exclusion, and hard sphere overlap. The system will crowd as close to the potential well as possible, but will not all be able to adsorb completely, as is seen in the snapshots (Figure 4.2).

The contact probability for the polymer network is seen in Figure 4.20. Panel (a) is given as a normalization over all chains, while (b) is normalized only over the chains which interact with the NP. For low values of k_{ang} (red solid line and orange dashed line) Figure 4.20(a) shows a slight increase in contact probability near the second to first and last monomers, indicating that the NP prefers to associate to the chains, close to the nodes. As angular potential increases, $k_{\text{ang}} = 0.006\,\text{kJ mol}^{-1}$ (indigo dash-dotted line) and $k_{\text{ang}} = 0.010\,\text{kJ mol}^{-1}$ (dark red dotted line) the probability increases for the center monomers, and decreases for the ends.

For $k_{\text{ang}} = 1.0\,\text{kJ mol}^{-1}$ the probability increases for monomers approximately four or five monomers from the end, as seen in Figure 4.20(b). As the polymer network is completely stiff, the NP maximizes interactions

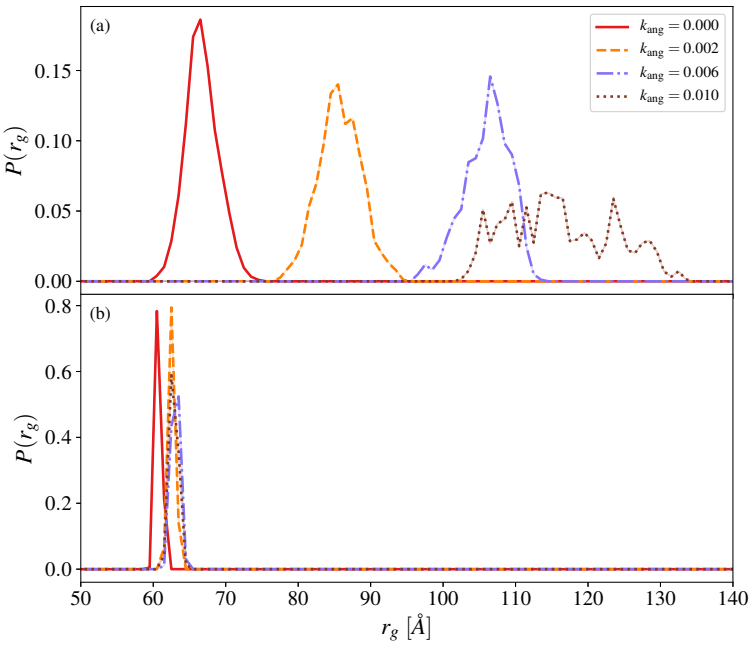

Figure 4.19: Probability distribution, $P(r_g)$, for the radial distribution, r_g, for the polymer network at varying chain stiffness, k_{ang}, when adsorbing to a nanoparticle. Panel (a) shows $P(r_g)$ for $\varepsilon/k_BT = 0.0$, and is treated as a reference for the gel, and (b) for $\varepsilon/k_BT = 1.0$. $g(r)$ for $k_{\text{ang}} = 1.0\,\text{kJ}\,\text{mol}^{-1}$ is not included as it did not change, and retained the value of $r_g = 200.0\,\text{Å}$ for both interaction strengths. Legends are shared between columns and the error (standard deviation) is included as a shadow in the same color as the corresponding line.

by adsorbing near the nodes. This is clear when viewing the snapshots of the system, and can be seen in Figure 4.2(e). The NP does not adsorb to the nodes themselves, which seems to be due to the strong repulsive forces for distances lower than σ for the LJ potential, and as such it sticks to the three chains in an attempt to increase interactions with monomers as much as possible. Throughout the simulation the NP seems to move around within the polymer network, close to the nodes.

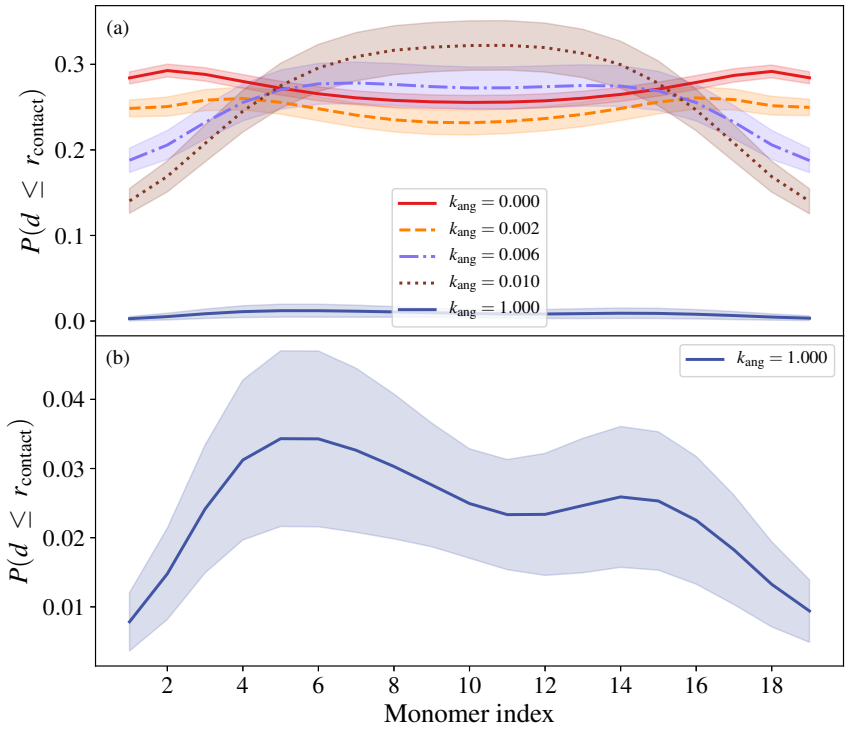

Figure 4.20: NP-monomer contact probability, $P(d \leq r_{\text{contact}})$, of given monomer for the polymer network at $\varepsilon/k_BT = 1.0$. The contact probability is normalized for all chains in contact in (a), while only for chains in contact with the nanoparticle in (b). The error (standard deviation) is included as a shadow in the same color as the corresponding line.

Chapter 5

Conclusion

5.1 Summary

The interaction between a NP and a restricted polymer chains or polymer network, have been studied. For the chains a varying degree of restrictions at and points, and at the middle, were used to mimic the interface topologies of a gel. Changing the separation of the nodes is assumed to have the same effect as swelling and de-swelling of a polymer network. For the polymer network, varying the stiffness of the chain was thought to induce the same effect.

When comparing a free chain to a chain with one node, there were no significant differences. At no interacting potential the free polymer chain showed a slightly larger probability of interacting randomly with the NP. For small potentials the polymer chain with one node showed a slightly lower probability of adsorbing to the NP.

For short node separations, all systems showed similar trends in regards to adsorption of the chain, and evolution of loops, tails and trains, with increasing potential. As the potential increases the length of loops, tails

and trains decreases. Similarly, the number of loops and trains, along with number of adsorbed segments, increases, while the number of tails decrease, for the same change. The system shows a tendency to favor many short tails and trains.

At node separations comparable to the diameter of the NP, the chain indicators diverge. For these systems, the number of tails increases to the maximum of 2.0 for low potentials and the number of loops and trains are not as sensitive to the changes in potential. For the three node system, the number and length of loops, tails and trains, is more sensitive to the small changes in nodes separation than for the other systems.

Regarding the NP-monomer contact probabilities, there is no difference between the free chain and one node system. For low separations the two node system behaves similarly to the one node system, but with a slight increase in probability of contact at the ends. As the separation increase, the contact probability at the end decreases, and the NP prefers the center of the chain. At extreme node separations, the distribution along the chain approximates a Gaussian distribution.

For the NP-monomer contact probability of the three node system, there is a higher probability of the NP adsorbing to the monomers next to the central node, but not at it. This seems to be the effect of steric repulsion due to monomer crowding at the central node. Also, the NP is shown to prefer to interact with either the first and central node, or the central and last node.

As the node separation increases, the NP adsorbs strongly to the central node, and the probability of finding it at the first or last monomer decreases to zero for lower separations than for the two node system. At node separations above twice that of the contact radius, the three node system shows a similar evolution as the two node system, and the NP

seems to prefer adsorbing to one chain.

Adsorption between the polymer network and NP show interesting results, and a variation on varying the stiffness of the polymers. Further investigation is needed to asses the action of contact, and evolution with degree of crosslinking and swelling.

5.2 Suggested further work

In this thesis, a simple single chain systems have been investigated. Increasing the complexity of these systems may prove valuable. By increasing the number of polymers perpendicular to the system, a system resembling the tetra-functional crosslinks of the polymer network is further approximated. Other interesting aspects may be to add charge to the system, and investigate the effects of chain stiffness in the node system. For the one node system, setting the node to be at a wall may be a way of probing the gel more accurately.

For the polymer network there are many possibilities. For the system with changing chain stiffness, an increase in intermediate values for the chain stiffness is needed. Other ways to asses the degree of swelling without restricting the chains is to add attractive or repulsive forces to the nodes. This may also prove valuable when looking at crosslinking density in comparison to swelling.

A polymer network with long chains and low node separations is comparable to an unswollen gel. Having the NP as an adhesive between two gels, the node separation has to be lower than the diameter of the NP for the NP to not get adsorbed in the gel. Adding attractive forces between nodes may prove an easy way to asses the adsorption for varying crosslinking density. This lets the chain retain the length and conforma-

tional freedom, in comparison to changing the stiffness of the chain to induce swelling, where the number of conformations are reduced when the chain is stiffer.

Finally, adding charges to the polymer network and NP may be of interest. Most biological polymers have some charge and the surface charge of the silica NP has been shown to be pH-dependent. Thus, assessing charges may prove usefull in comparison to the *in vivo* system.

Bibliography

Adili, A., Crowe, S., Beaux, M. F., Cantrell, T., Shapiro, P. J., McIlroy, D. N. & Gustin, K. E. (2008), 'Differential cytotoxicity exhibited by silica nanowires and nanoparticles', *Nanotoxicology* **2**(1), 1–8.

Annabi, N., Tamayol, A., Shin, S. R., Ghaemmaghami, A. M., Peppas, N. A. & Khademhosseini, A. (2014), 'Surgical materials: current challenges and nano-enabled solutions', *Nano today* **9**(5), 574–589.

Barisik, M., Atalay, S., Beskok, A. & Qian, S. (2014), 'Size dependent surface charge properties of silica nanoparticles'.

Bitsanis, I. A. & Brinke, G. t. (1993), 'A lattice monte carlo study of long chain conformations at solid–polymer melt interfaces', *The Journal of chemical physics* **99**(4), 3100–3111.

Brunel, B., Beaune, G., Nagarajan, U., Dufour, S., Brochard-Wyart, F. & Winnik, F. M. (2016), 'Nanostickers for cells: a model study using cell–nanoparticle hybrid aggregates', *Soft matter* **12**(38), 7902–7907.

Choi, Y., Lee, J. E., Lee, J. H., Jeong, J. H. & Kim, J. (2015), 'A biodegradation study of sba-15 microparticles in simulated body fluid and in vivo', *Langmuir* **31**(23), 6457–6462.

Christiansen, N. (2017), 'Monte carlo simulations to probe the gel-nanoparticle-gel interface'. Technical report, NTNU, Trondheim.

Clark, A. H. & Ross-Murphy, S. B. (1987), Structural and mechanical properties of biopolymer gels, *in* 'Biopolymers', Springer, pp. 57–192.

Cosgrove, T. (2010), *Colloid science: principles, methods and applications*, John Wiley & Sons.

Devasena, T. (2016), *Therapeutic and Diagnostic Nanomaterials*, Springer.

Fleer, G. & Scheutjens, J. (1982), 'Adsorption of interacting oligomers and polymers at

an interface', *Advances in Colloid and Interface Science* **16**(1), 341–359.

Flory, P. J. (1953), *Principles of polymer chemistry*, Cornell University Press.

Gao, Y., Han, Y., Cui, M., Tey, H. L., Wang, L.-H. & Xu, C. (2017), 'Zno nanoparticles as an antimicrobial tissue adhesive for skin wound closure', *Journal of Materials Chemistry B* .

Guzman, E., Ortega, F., Baghdadli, N., Cazeneuve, C., Luengo, G. S. & Rubio, R. G. (2011), 'Adsorption of conditioning polymers on solid substrates with different charge density', *ACS applied materials & interfaces* **3**(8), 3181–3188.

Hao, N., Liu, H., Li, L., Chen, D., Li, L. & Tang, F. (2012), 'In vitro degradation behavior of silica nanoparticles under physiological conditions', *Journal of nanoscience and nanotechnology* **12**(8), 6346–6354.

Haraguchi, K. (2007), 'Nanocomposite hydrogels', *Current Opinion in Solid State and Materials Science* **11**(3-4), 47–54.

Haraguchi, K. & Li, H.-J. (2006), 'Mechanical properties and structure of polymer- clay nanocomposite gels with high clay content', *Macromolecules* **39**(5), 1898–1905.

Hardin, J. & Bertoni, G. P. (2015), *Becker's World of the Cell*, eighth edn, Pearson.

Huang, X., Teng, X., Chen, D., Tang, F. & He, J. (2010), 'The effect of the shape of mesoporous silica nanoparticles on cellular uptake and cell function', *Biomaterials* **31**(3), 438–448.

Källrot, N. & Linse, P. (2010), 'Dynamics of competitive polymer adsorption onto planar surfaces in good solvent', *The Journal of Physical Chemistry B* **114**(11), 3741–3753.

Kim, J.-H., Kim, H., Choi, Y., Lee, D. S., Kim, J. & Yi, G.-R. (2017), 'Colloidal mesoporous silica nanoparticles as strong adhesives for hydrogels and biological tissues', *ACS applied materials & interfaces* **9**(37), 31469–31477.

Lesniak, A., Salvati, A., Santos-Martinez, M. J., Radomski, M. W., Dawson, K. A. & Åberg, C. (2013), 'Nanoparticle adhesion to the cell membrane and its effect on nanoparticle uptake efficiency', *J. Am. Chem. Soc* **135**(4), 1438–1444.

Li, L., Liu, T., Fu, C., Tan, L., Meng, X. & Liu, H. (2015), 'Biodistribution, excretion, and toxicity of mesoporous silica nanoparticles after oral administration depend on their shape', *Nanomedicine: Nanotechnology, Biology and Medicine* **11**(8), 1915–1924.

Liu, H., Peng, Y., Yang, C. & Wang, M. (2017), 'Silica nanoparticles as adhesives for biological tissues? re-examining the effect of particles size, particle shape, and the unexpected role of base', *Particle & Particle Systems Characterization* **34**(12), 1700286.

Meddahi-Pellé, A., Legrand, A., Marcellan, A., Louedec, L., Letourneur, D. & Leibler,

L. (2014), 'Organ repair, hemostasis, and in vivo bonding of medical devices by aqueous solutions of nanoparticles', *Angewandte Chemie International Edition* **53**(25), 6369–6373.

Moia, C. (2015), In vitro toxicological assessment of amorphous silica particles in relation to their characteristics and mode of action in human skin cells, PhD thesis, Cranfield University.

Murthy, S. K. (2007), 'Nanoparticles in modern medicine: state of the art and future challenges', *International journal of nanomedicine* **2**(2), 129.

Napierska, D., Thomassen, L. C., Rabolli, V., Lison, D., Gonzalez, L., Kirsch-Volders, M., Martens, J. A. & Hoet, P. H. (2009), 'Size-dependent cytotoxicity of monodisperse silica nanoparticles in human endothelial cells', *Small* **5**(7), 846–853.

Nelson, D. L. & Cox, M. M. (2013), *Lehninger Principles of Biochemistry*, sixth edn, WH Freeman & Co.

Noguchi, H. & Takasu, M. (2002), 'Adhesion of nanoparticles to vesicles: a brownian dynamics simulation', *Biophysical journal* **83**(1), 299–308.

Næss, S. N., Mikkelsen, A., Elgsæter, A. & de Sousa Dias, R. (2016), *Molecular Biophysics*, Norwegian University of Science and Technology[Host].

Perrin, E., Schoen, M., Coudert, F.-X. & Boutin, A. (2018), 'Structure and dynamics of solvated polymers near a silica surface: On the different roles played by solvent', *The Journal of Physical Chemistry B* **122**(16), 4573–4582.

Reščič, J. & Linse, P. (2015), 'Molsim: A modular molecular simulation software', *Journal of computational chemistry* **36**(16), 1259–1274.

Rose, S., Prevoteau, A., Elziere, P., Hourdet, D., Marcellan, A. & Leibler, L. (2014), 'Nanoparticle solutions as adhesives for gels and biological tissues', *Nature* **505**(7483), 382.

Sariban, A. & Binder, K. (1987), 'Critical properties of the flory–huggins lattice model of polymer mixtures', *The Journal of chemical physics* **86**(10), 5859–5873.

Scheutjens, J. & Fleer, G. (1980), 'Statistical theory of the adsorption of interacting chain molecules. 2. train, loop, and tail size distribution', *The Journal of Physical Chemistry* **84**(2), 178–190.

Shibayama, M., Suda, J., Karino, T., Okabe, S., Takehisa, T. & Haraguchi, K. (2004), 'Structure and dynamics of poly (n-isopropylacrylamide)- clay nanocomposite gels', *Macromolecules* **37**(25), 9606–9612.

Simha, R., Frisch, H. & Eirich, F. (1953), 'The adsorption of flexible macromolecules', *The Journal of Physical Chemistry* **57**(6), 584–589.

Smith, J. S., Bedrov, D. & Smith, G. D. (2003), 'A molecular dynamics simulation study of nanoparticle interactions in a model polymer-nanoparticle composite', *Composites science and technology* **63**(11), 1599–1605.

Song, Q., Ji, Y., Li, S., Wang, X. & He, L. (2018), 'Adsorption behavior of polymer chain with different topology structure at the polymer-nanoparticle interface', *Polymers* **10**(6), 590.

Stornes, M., Linse, P. & Dias, R. S. (2017), 'Monte carlo simulations of complexation between weak polyelectrolytes and a charged nanoparticle. influence of polyelectrolyte chain length and concentration', *Macromolecules* **50**(15), 5978–5988.

Theng, B. K. G. (1982), 'Clay–polymer interactions: summary and perspectives', *Clays and Clay Minerals* pp. 1–10.

Thompson, R. B., Ginzburg, V. V., Matsen, M. W. & Balazs, A. C. (2001), 'Predicting the mesophases of copolymer-nanoparticle composites', *Science* **292**(5526), 2469–2472.

Treloar, L. R. G. (2005), *The physics of rubber elasticity*, third edn, Oxford University Press, USA.

Welch, D., Lettinga, M., Ripoll, M., Dogic, Z. & Vliegenthart, G. A. (2015), 'Trains, tails and loops of partially adsorbed semi-flexible filaments', *Soft matter* **11**(38), 7507–7514.

Wu, J., Wang, C., Sun, J. & Xue, Y. (2011), 'Neurotoxicity of silica nanoparticles: brain localization and dopaminergic neurons damage pathways', *ACS nano* **5**(6), 4476–4489.

Yoon, Y.-E., Im, B. G., Kim, J.-s. & Jang, J.-H. (2016), 'Multifunctional self-adhesive fibrous layered matrix (film) for tissue glues and therapeutic carriers', *Biomacromolecules* **18**(1), 127–140.

Appendix A

Additional figures

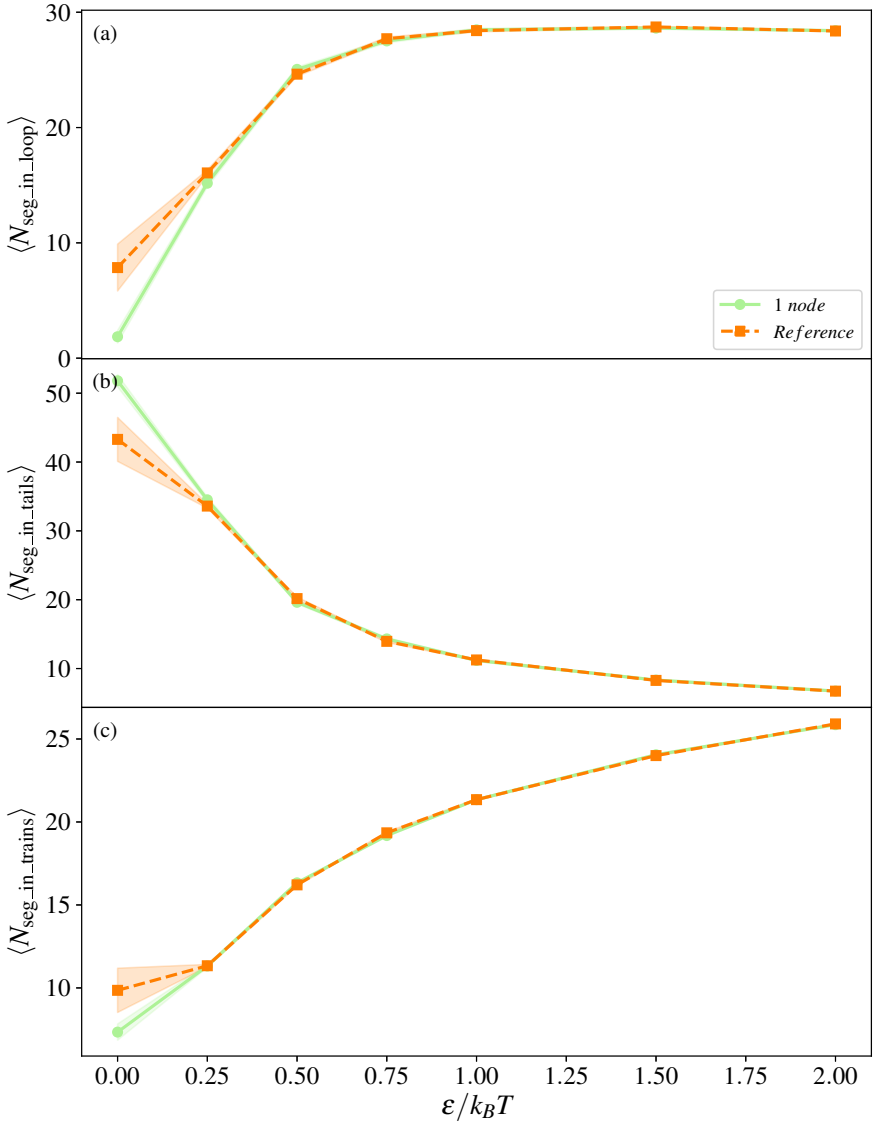

Figure A.1: Average number of segments, $\langle N_\alpha \rangle$, in loops, tails and trains for system 1 and the reference system. α denotes loops, tails and trains respectively. Legends are shared between columns and the error (standard deviation) is included as a shadow in the same color as the corresponding line.

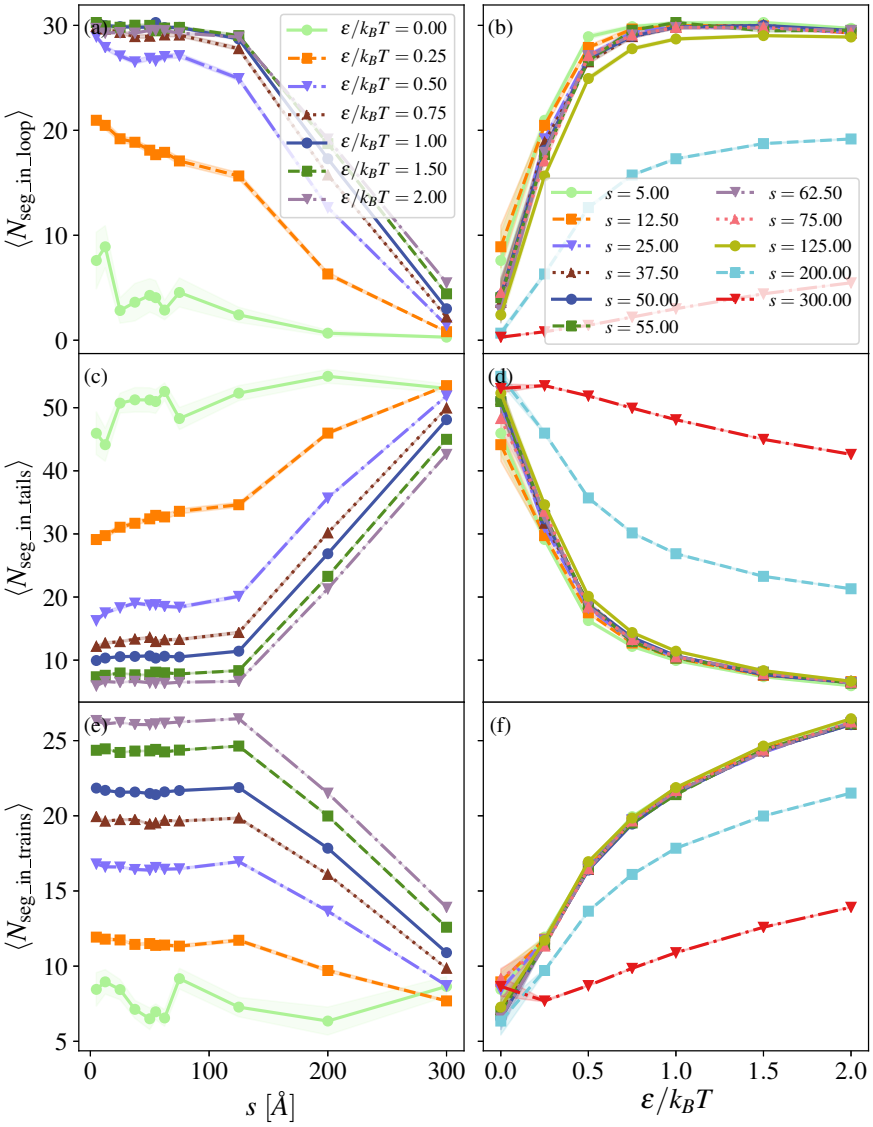

Figure A.2: Average number of segments, $\langle N_\alpha \rangle$, in loops, tails and trains for system 2. Panels (a), (c) and (e) show loops, tails and trains as a function of node separation, s. (b), (d) and (f) show loops, tails and trains as a function of potential, ε/k_BT. α denotes loops, tails and trains respectively. Legends are shared between columns.

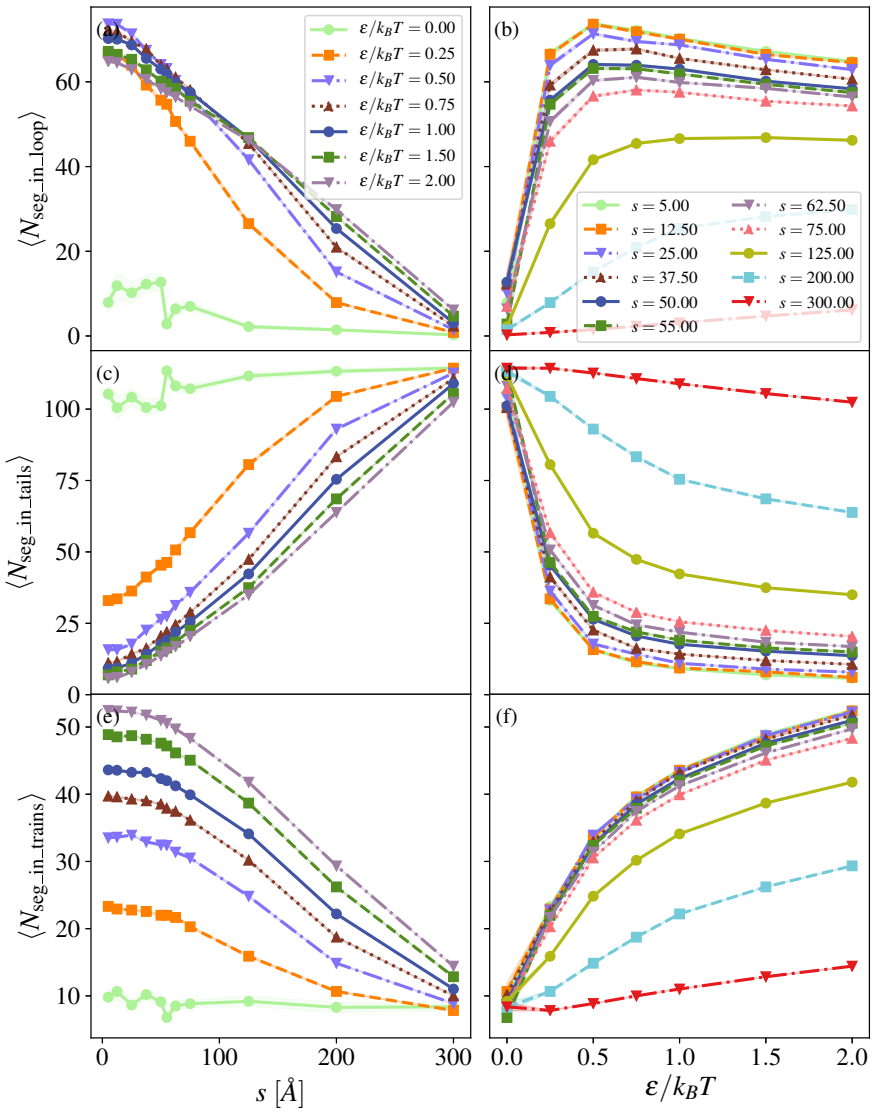

Figure A.3: Average number of segments, $\langle N_\alpha \rangle$, in loops, tails and trains for system 3. Panels (a), (c) and (e) show loops, tails and trains as a function of node separation, s. (b), (d) and (f) show loops, tails and trains as a function potential, ε/k_BT. α denotes loops, tails and trains respectively. Legends are shared between columns and the error (standard deviation) is included as a shadow in the same color as the corresponding line.

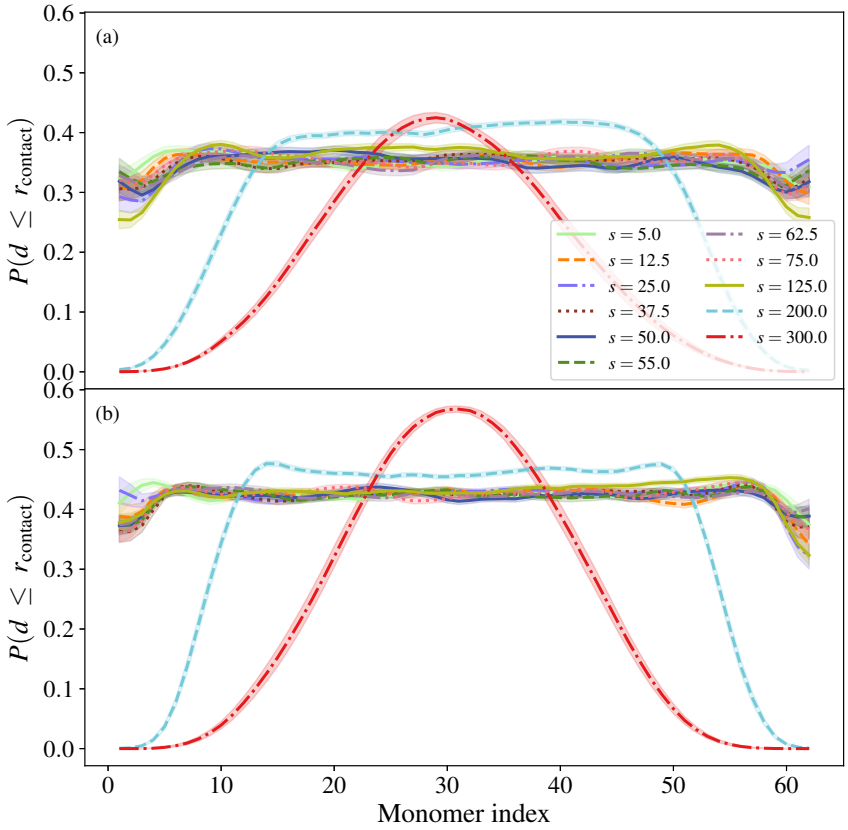

Figure A.4: NP-monomer contact probability, $P(d \leq r_{\text{contact}})$, of a given monomer for 2 nodes for $\varepsilon/k_BT = 1.0$ (a) and $\varepsilon/k_BT = 2.0$ (b), at varying node separation, s. Legends are shared between columns and the error (standard deviation) is included as a shadow in the same color as the corresponding line.

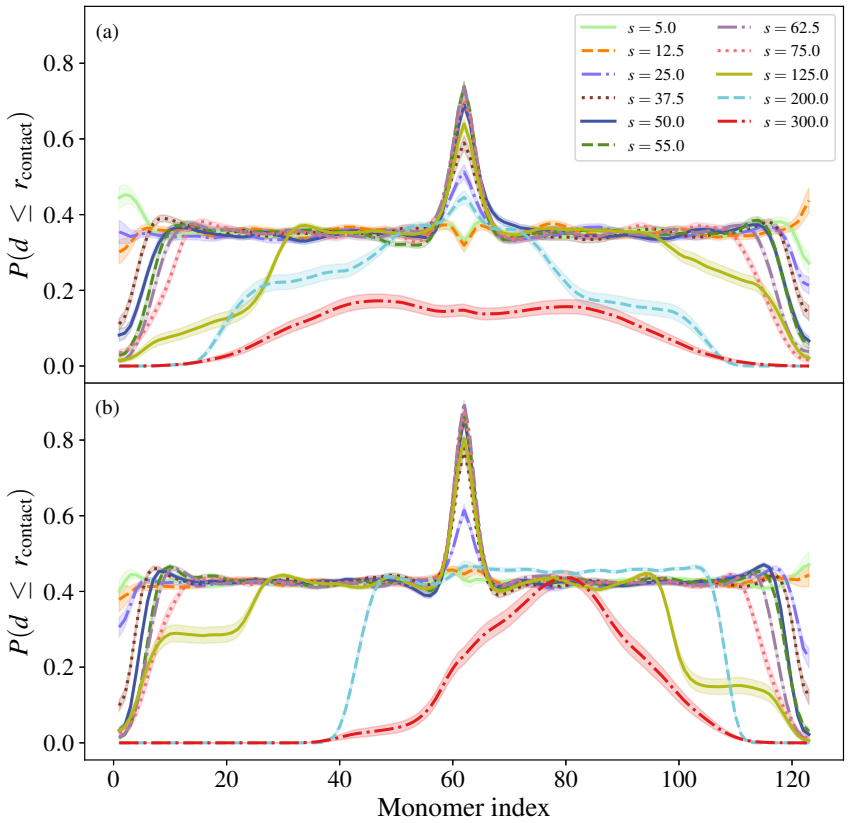

Figure A.5: NP-monomer contact probability, $P(d \leq r_{\text{contact}})$, of given monomer for 2 nodes for $\varepsilon/k_BT = 1.0$ (a) and $\varepsilon/k_BT = 2.0$ (b), at varying node separation, s. Legends are shared between columns and the error (standard deviation) is included as a shadow in the same color as the corresponding line.

Appendix B

Input files

System file for the single chain with three nodes interacting with a NP. To be used as input in *MOLSIM*.

```
&nmlSystem
 txtitle ='One NP and two 60 monomer chain connected to three
   nodes'
 txmode='simulation',
 txmethod='mc',    txensemb='nvt',     txbc='sph',
   txstart='zero',
 nstep1= 100,        nstep2= 45000,
 sphrad= 600.0,
 temp  = 298.0,    prsr = 0.1013,
 iseed = 1,
 lcont =.t.,  laver =.t.,  ldist =.t., ldump =.f., lgroup=.f.,
     lstatic =.t.,  limage=.t.
 itest = 0,   ipart = 0,   iatom = 1,   iaver = 0,   ishow =
   1,     iplot = 1,   ilist = 1,
/
&nmlScale
/
&nmlParticle
```

```
 nct    = 1,
 txct   ='2x2x60-mer+3-node',
 ncct   = 1,
 npptct(1:2,1) = 3,120,
 nblockict(1) = 2,
 txcopolymer = 'repeating',
 npt    = 3,
 txpt   = 'node', 'mon', 'np',
 nppt   =  3,   120,    1,
 natpt  =  1, 1,  1,
 txat   = 'node', 'bead', 'np',
 radat  =  2.0,  2.0, 50.0,
 naatpt(1,1) =  1,
 txaat(1,1) = 'node',
 naatpt(1,2) = 1,
 txaat(1,2) = 'bead',
 naatpt(1,3) = 1,
 txaat(1,3) = 'np',
 sigat(1) = 61.7,
 epsat(1) = 2.480,
 sigat(2) = 61.7,
 epsat(2) = 2.480,
 sigat(3) = 61.7,
 epsat(3) = 2.480,
 lradatbox = .t.,
 nodesep = 55.00,
/
&nmlRepeating
 rep_iblock_ict(1:2,1)%pt = 1,2,
 rep_iblock_ict(1:2,1)%np = 1,60,
 /
&nmlPotential
 rcut = 0.0,
 txpot(3) = '(1,6,12)',
 txpot(5) = '(1,6,12)',
```

```
50   relpermitt = 78.4,
51  /
52  &nmlPotentialChain bond = 2.4088, 2, 5.0, angle = 0.002/
53  &nmlSetConfiguration txsetconf =  'oneturn', 'oneturn', '
       random', anglemin = 0.0 /
54  &nmlMC
55   pspart = 0.0, 1.0, 1.0,  dtran      = 0.0, 5.0, 5.0,
56   pchain = 0.0, 0.0, 0.0,       dtranchain = 0.0, 0.0,
57   ppivot = 0.0, 0.0,  drotpivot  = 360.0, 360.0,
       ipivotrotmode = 1,
58   itestmc = 0,
59   lfixzcoord(1) = .f.,
60   lfixxycoord(1) = .f.,
61  /
62  &nmlDump
63   idump =100,
64   txptdump='all',
65   ldpos =.t.,
66   ldori =.f.,
67   ldfor =.f.,
68   ldtor =.f.,
69   ldidm =.f.,
70 /
71  &nmlStatic
72   istatic = 1,
73   lchaintypedf = .t.,
74   lcbpc = .t.,
75   lltt = .t.,
76   lmeanforce1 = .f.,
77   lenergydf = .f.,
78   lrdfsph = .f.
79  /
80  &nmlChainTypeDF vtype(2) =.true., 0.0, 350., 350, vtype(3) = .
       true., 0.0, 350., 350 /
81  &nmlCBPC iptpart = 3, rcontact = 70.0, /
```

```
&nmlLoopTailTrain adscond= 'part=124', , 70.0d0 /
&nmlIntList inlist = 0, drnlist = 2600.0,   facnneigh = 50.0 /
&nmlDist idist = 10, vtype(5) =.true., 0.0, 350.0, 350 /
&nmlImage lvrml =.false., lvtf = .true./
&nmlVRML txwhen='after_macro', blmax = 5.0, bondr = 0.3 /
&nmlVTF txfile = 'split', txwhen='after_macro', blmax = 5.0,
   bondr = 0.3, bondres = 50, sphres = 50, lframezero = .true.
    /
```

System file for the gel and single NP.

```
&nmlSystem
 txtitle   = 'single microgel plus np layer',
 txmode    = 'simulation',
 txmethod  =         'mc',
 txensemb  =        'nvt',
 txbc      =        'sph',
 txstart   =    'continue',
 sphrad    =       600.0 ,
 temp      =      298.15 ,
 prsr      =       1.013 ,
 iseed     =           1 ,
 nstep1    =         100 ,
 nstep2    =       60000 ,
 lcont     = .t.,  laver = .t.,  ldist = .t.,  ldump = .f.,
   lgroup = .t.,  lstatic = .t.,  ldynamic = .f.,  limage = .t
   . ,
 itest     =  0 ,  ipart =  1 ,  iatom =  1 ,  iaver =  0 ,
   ishow  =  1 ,  iplot   =  1 ,  ilist    =  1 ,  ltrace = .f
   . ,
 lblockaver = .f.,
/
&nmlScale
/
&nmlParticle
 lclink        =       .true.,
```

```
22 nnwt          =          1 ,
23 nct           =          1 ,
24 txct(1)       =   'strand_T',
25 ncct(1)       =         88 ,
26 npt           =          3 ,
27 txpt(1)       =     'node_T', txpt(2)       = 'monT',   txpt
   (3)       =   'np',
28 nppt(1)       =         35 , nppt(2)       =  1672 ,   nppt
   (3)       =     1 ,
29 natpt(1)      =          1 , natpt(2)      =     1 ,   natpt
   (3)       =     1 ,
30 txat(1)       =     'node_T', txat(2)       = 'monT',   txat
   (3)       =   'np',
31 radat(1)      =        2.0 , radat(2)      =   2.0 ,   radat
   (3)       =  40.0 ,
32 npptct(1,1)   =          0 , npptct(2,1)   =    19 ,   npptct
   (3,1)   =     0 ,
33 zat(1)        =        0.0 , zat(2)        =   0.0 ,   zat(3)
          =   0.0 ,
34 maxnbondcl(1) =          4 , maxnbondcl(2) =     1 ,
   maxnbondcl(3) =     0 ,
35 naatpt(1,1)   =          1 , naatpt(1,2)   =     1 ,   naatpt
   (1,3)   =     1 ,
36 txaat(1,1)    =     'node_T', txaat(1,2)    = 'monT',   txaat
   (1,3)    =   'np',
37 sigat(1)      =      49.84 , sigat(2)      = 49.84 ,   sigat
   (3)       = 49.84 ,
38 epsat(1)      =       2.4800 , epsat(2)      =  2.4800 ,
   epsat(3)      =  2.4800 ,
39 itestpart = 10
40 lradatbox = .t.,
41 /
42 &nmlNetworkConfiguration
43 nnwnwt(1)     =          1 ,
44 iptclnwt(1)   =          1 ,
```

```
 nctnwt(1,1)  =          88 ,
 txnwt(1)     = 'microgel_T',
 txtoponwt(1) =    'default',
/
&nmlPotential
relpermitt =  78.3 ,
lewald     =    .f.,
txewaldrec =  'std',
iewaldopt  =     1 ,
rcut       =   0.0 ,
txpot(3) = '(1,6,12)', txpot(5) = '(1,6,12)',
/
&nmlPotentialChain
 bond(1)  = 2.4088, 2, 5.0,
 angle(1) = .006,
 clink    = 2.4088, 2, 5.0,
/
&nmlSetConfiguration
 rnwt(1)         =    250.0 ,
 txoriginnwt(1)  =  'origin',
 txsetconf(1)    = 'network', txsetconf(3)    = 'random',
 txsetconf(2)    = 'network',
 rcupp(3,3)      =  -300.00 ,
/
&nmlMC
 isamp = 1,
 pspart(1)  = 1.00 , pspart(2)  = 1.00 , pspart(3)  = 1.00,
 dtran(1)   = 5.00 , dtran(2)   = 5.00 , dtran(3)   = 5.00 ,
 ppivot = 0.0, 0.0, 0.0,  drotpivot  = 360.0, 360.0,
    ipivotrotmode = 1,
 itestmc = 0,
 lfixzcoord(1) = .f.,
 lfixxycoord(1) = .f.,
/
&nmlIntLis
```

```
 inlist  =    0 ,
 drnlist =  950 ,
/
&nmlStatic
istatic           =  1 ,
lchaintypedf      = .t.,
lcbpc             = .t.,
lltt              = .t.,
lmeanforce1       = .f.,
lenergydf         = .f.,
lrdfsph           = .f.,
lnetworkdf        = .t.,
lnetworkradialdf  = .t.,
/

&nmlNetworkDF
 vtype(1) = .t., 0.0, 300.0, 300,
 vtype(2) = .t., 0.0, 0.010, 100,
/
&nmlNetworkRadialDF
 vtype(1) = .t., 0.0, 500.0, 500,
 vtype(2) = .t., 0.0, 100.0, 200,
 vtype(3) = .t., 0.0, 500.0, 500,
 vtype(7) = .t., 0.0, 500.0, 500,
/

&nmlImage
 iimage =  5 ,
 lvtf   = .t.,
 lvrml =.f.,
/
&nmlVTF
 txwhen  = 'after_macro',
 txfile = 'split',
 blmax = 5.0,
```

```
 bondr    =          0.3  ,
 bondres =           50  ,
 sphres   =          50  ,
 tximage = 'frame','','',

 lframezero = .true. /

&nmlChainTypeDF vtype(2) =.true., 0.0, 120., 120, vtype(3) = .
    true., 0.0, 100., 100 /

&nmlCBPC
iptpart =      3,
rcontact = 56.57,
/
&nmlLoopTailTrain adscond= 'part=3568', , 56.57d0, /
&nmlIntList inlist = 0, drnlist = 2600.0,   facnneigh = 50.0 /
&nmlDist idist = 10, vtype(5) =.true., 0.0, 300.0, 300/


&nmlVRML
txwhen='after_macro',
blmax = 5.0,
bondr = 0.3,
txfile = 'separated',
/
```